



Research of on-line monitoring technology and control strategy for laser-directed energy deposition: a review

Weiwei Liu^{1,2,3} · Tandong Wang^{1,2} · Bingjun Liu^{1,2} · Wanyang Li^{1,2} · Guangda Hu^{1,2} · Zhenxin Lyu^{1,2}

Received: 24 August 2023 / Accepted: 27 May 2024 / Published online: 18 June 2024
© The Author(s), under exclusive licence to Springer-Verlag London Ltd., part of Springer Nature 2024

Abstract

As an advanced metal additive manufacturing technology, laser-directed energy deposition (DED-LB) has attracted a lot of attention in recent years, and is increasingly used in aerospace, automotive, marine, and biomedical applications. However, as industry application standards continue to improve, the challenges of part quality, process stability, and molding efficiency faced by DED-LB are becoming more and more prominent. On-line monitoring and real-time quality regulation can effectively avoid quality defects in processing, which is an effective measure to solve the problem. This paper summarizes the current research status of on-line monitoring means and closed-loop quality regulation technology for DED-LB. The on-line monitoring signals and related sensing devices mainly based on image signals, temperature signals, spectral signals, acoustic emission signals, and X-ray imaging, as well as the closed-loop control strategies and intelligent optimization methods in the process are discussed. Finally, a view on the future direction of on-line monitoring-control system for DED-LB is presented.

Keywords Laser-directed energy deposition · On-line monitoring technology · Control strategies · Optimization methods · On-line monitoring-control system

1 Introduction

As the mainstay of the national economy, the manufacturing industry has been seeking new methods and technologies to improve productivity and product quality while reducing manufacturing costs in recent years. As an innovative technology in the actual manufacturing industry, laser additive manufacturing (LAM) forms a bottom-up processing by melting metal powder or wire layer by layer [1], and is gradually being widely used. With the development of science and technology, its connotation is being deepened and its extension is being fully expanded. According to the different

material treatment methods, laser additive manufacturing can be divided into selective laser melting (SLM), laser-directed energy deposition (DED-LB) [2], etc. The problem of low productivity of SLM [3] has led to its failure to be widely used in industrial production.

DED-LB is one of the most commonly used cladding method based on laser surface modification [4], often also referred to as laser cladding (LC) [5]. A high-energy laser beam is utilized to rapidly melt the coating material and the substrate to form a 50- μm 2-mm thick bonding layer [6, 7]. Thereby, the surface volume of the substrate is not altered and very low dilution rates are guaranteed [8]. According to the different ways of powder entering the deposition layer, the two methods of pre-positioned powder and coaxial powder feeding are commonly used [9–11]. In general, the pre-positioned powder system is easy to operate and has a better quality of deposition, but the depth of deposition is difficult to control. The coaxial powder feeding system has higher laser utilization [12], but the process involves the coupling of multiple physical fields such as material, laser, optics, powder, and airflow [13], such multi-parameters make it more controllable [14]. Most of the DED-LB process control methods described in this paper are based on coaxial powder feeding systems, and the DED-LB system is shown

✉ Weiwei Liu
liuww@dlut.edu.cn

✉ Tandong Wang
wtddlut@163.com

¹ School of Mechanical Engineering, Dalian University of Technology, Dalian 116024, China

² State Key Laboratory of High-Performance Precision Manufacturing, Dalian University of Technology, Dalian 116024, China

³ Ningbo Institute of Dalian University of Technology, Ningbo 315000, China

in Fig. 1 [15]. DED-LB has the following advantages over other processes:

- (1) DED-LB is able to form a more homogeneous and dense high-quality deposition layer between the metal powder and the substrate compared to TIG welding. Sexton et al. [16] verified this advantage in terms of dilution rate and hardness in repairing the blades of a turbojet engine.
- (2) Based on its technological mechanism, DED-LB is able to be applied to a wide range of materials such as metal alloys [7] and composites [17]. Bartkowski et al. [17] verified the microhardness and corrosion resistance of metal matrix composite (MMC) coatings prepared by DED-LB.
- (3) DED-LB is a rapid melting and rapid cooling process that produces a smaller heat-affected zone. This results in grain refinement [18] and reduces the effects of thermal damage and material deformation [8].

The above characteristics make DED-LB attractive in the field of surface engineering [7, 18, 19]. It is often applied to surface coating, repair and rapid prototyping in aerospace [20], automotive marine [21], and biomedical [22]. DED-LB is an integration of greening, automation, and personalization that enables efficient production while reducing material waste, which is in line with contemporary manufacturing needs and trends.

Although significant progress has been made in DED-LB technology, it is undeniable that there are still many challenges and technical limitations. Since DED-LB is a multi-field, multi-parameter coupled complex physical, chemical, and metallurgical process [14], laser power, scanning speed, powder feeding rate, laser beam spot size, and protective gas and other small changes in any one of the parameters will directly affect the melt pool, powder flow, the transient process characteristics of the matrix, and further effect on the macro-form, microstructure, and mechanical properties of the formed parts. Specifically, it is mainly limited to the following issues [23–25]:

- (1) Numerical simulation can help to better understand the DED-LB process and derive data from it. However, idealized data does not really make sense to meet the increasing demands for quality control and assurance.
- (2) DED-LB is accompanied by real-time changes in the state of the material, which produces inconsistencies in the results. For example, melting or cooling rates that are too fast or too slow tend to produce more defects and residual stresses.
- (3) Process parameters have an important influence on the quality of DED-LB, but the complexity of the process and the nonlinear correlation between the quality of DED-LB and different process parameters make it difficult to determine the optimal combination of process parameters.

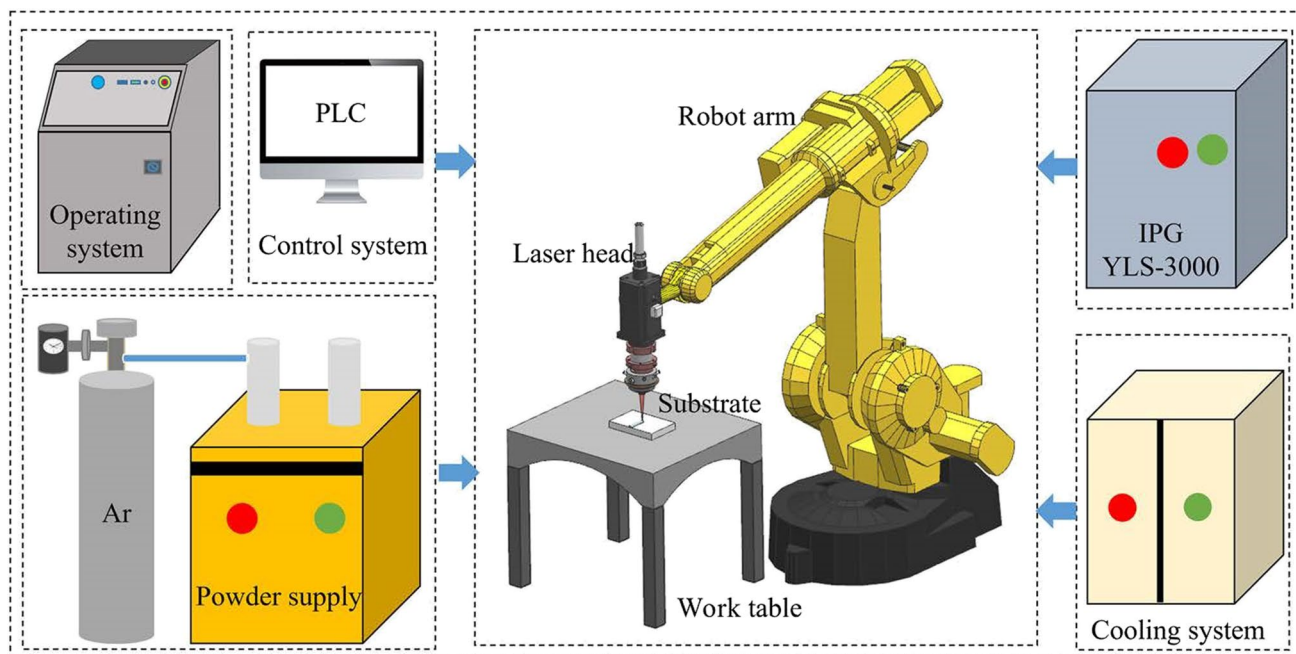


Fig. 1 Laser-directed energy deposition system [15]

In order to solve these problems, further optimize the deposition process, and improve the stability of DED-LB, researchers have been exploring and developing on-line monitoring methods and control strategies for the DED-LB process. As shown in Fig. 2, the number of publications in recent years shows that the topic of on-line monitoring and control of DED-LB has been growing in popularity year by year, which is a reflection of the importance of this type of research. At the present stage, the on-line monitoring means of the DED-LB process is mainly based on the dynamic characteristics of the melt pool and powder flow. The main monitoring signals are image signals based on morphology and size, temperature signals, as well as plasma spectral signals and acoustic emission signals [26], etc. Through on-line monitoring means, the process of interaction between laser, powder, and melt pool can be analyzed and restored. At the same time, a three-dimensional mapping relationship between process parameters, monitoring information, and molding quality is established, providing more basis for quality regulation. In addition, through the closed-loop control in the process, immediate response can be made when relevant defects are found and recognized, avoiding quality problems caused by inappropriate process parameters.

Therefore, on-line monitoring and real-time quality control are of great significance for the optimization and stability of the quality of the deposition layer, production efficiency, and the guarantee of reproducibility.

This paper summarizes the current research progress of on-line monitoring means and control strategies for DED-LB process. The principles, application effects, and main problems of various methods are discussed. Finally, on the basis of the existing methods, we put forward our views on the future development direction of the on-line monitoring system and control system for DED-LB.

2 On-line monitoring methods for DED-LB

DED-LB involves more than 19 process parameters [27], such as laser power, scanning speed, powder mass flow rate, and laser beam spot diameter. It is necessary to fully understand the relationship between different process parameters and forming quality in order to further optimize the quality of the deposition layer (Table 1). Conventional offline monitoring including metallographic microscopy, scanning electron microscopy (SEM) analysis, and non-destructive

Fig. 2 Number of papers on online monitoring and feedback control of directed energy deposition in Web of Science. Search was done using the topics “Laser Directed Energy Deposition” OR “Laser Cladding” AND “On-line monitoring” and “Laser Directed Energy Deposition” OR “Laser Cladding” AND “Feedback control”

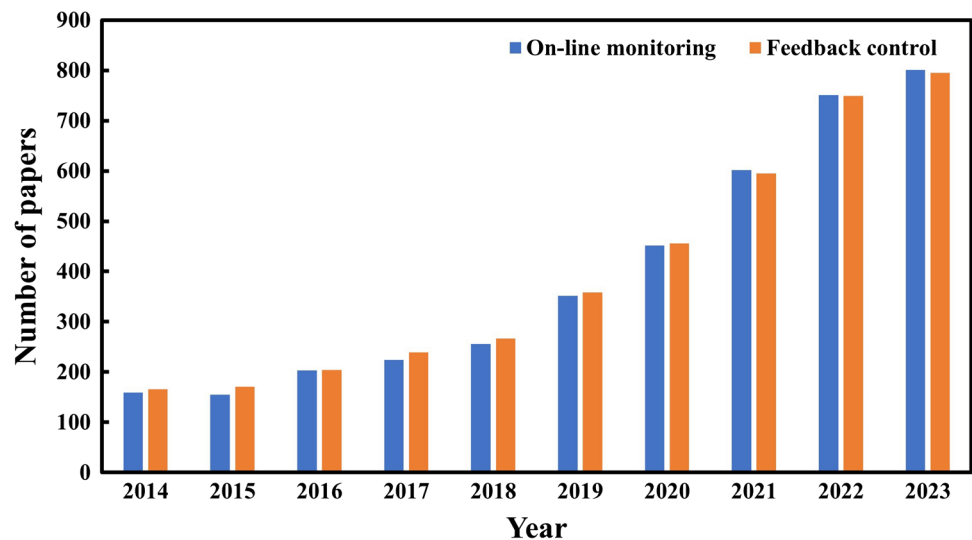


Table 1 Performance parameters of different types of pyrometers

Parameters	Contact type	Non-contact type		
	Thermocouples	Single-spot monochromatic pyrometer	Dual-color pyrometer	Infrared camera
Model number	CS-SF15-C1	CTLM-2HCF3-C3H	-	FLIR A655sc
Temperature range (°C)	0-1030	385–1600	1000–3000	-40-650
Spatial resolution	< 1 mm (0D)	0.7 mm (0D)	0D	15 × 10 mm ² (2D)
Sampling time (ms)	50	1	10	20
Wavelength (µm)	-	1.6	1.3, 1.64	0.9–1.7
Publications	[32]	[33]	[34, 35]	[36]

ultrasonic testing [28–31] can provide an assessment of the quality and performance of the formed parts. However, such methods can lead to interruptions and delays. The inability to provide real-time feedback on the deposition leads to the inability to achieve higher quality and efficiency. In contrast, on-line monitoring can provide real-time non-destructive performance evaluation. Therefore, researchers are continuously exploring and developing different on-line monitoring techniques to achieve real-time control and optimization of the deposition process.

In this section, the focus will be on different monitoring means in DED-LB technology. The types, characteristics,

and effectiveness of the sensors used in the different monitoring means are explored and compared. At the end of this section, information on the application of each type of monitoring signal is summarized in Table 2. In addition, a comparison of the five on-line monitoring methods presented is summarized in Table 3.

2.1 Morphology and size-based image monitoring methods

With the development of computer vision, machine vision, and image processing techniques, visualized image signals

Table 2 Summary of application information for on-line monitoring signals

Monitoring devices	Monitoring objects	Geometry	Powder	Substrates	Publications
CMOS camera	Melt pool width	Single layer	MetcoClad 52052	Inconel 718	[37]
CMOS camera	Melt pool width	Multi-	Stellite 5	4CrMo4	[38]
CMOS camera	Melt pool width	Single layer	EN25	-	[39]
CMOS camera	Melt pool width	Single layer	1.2344	1.2344	[40]
CCD camera	Height of deposition layer	Horseshoe-shaped part	SS316	SS10	[41]
CCD camera	Height of deposition layer	Cylinder	316L	SS304	[33]
CCD camera	Height of deposition layer	Multi-	316L	SS10L	[42]
CCD camera	Powder flight speed	Multi tracks and single layer	Ti-6Al-4V	S235	[43]
Single-spot monochromatic pyrometer	Melt pool temperature	Single layer	Inconel 718	AISI 304 austenitic steel	[44]
Single-spot monochromatic pyrometer	Melt pool temperature	Single layer	Inconel 718, TiC	AISI 304 austenitic steel	[45, 46]
Dual-color pyrometer	Melt pool temperature	Multi tracks and multi layers	H13	Carbon steel	[47]
Infrared camera	Melt pool temperature	Multi layers	Inconel 625	U75V, U20Mn	[48]
Infrared camera	Melt pool temperature	Multi layers	Ti-6Al-4V	Ti-6Al-4V	[49]
Type K thermocouple	Substrate temperature	Multi tracks and multi layers	Stellite 6, Inconel 625	SS316	[50]
Type K thermocouple	Substrate temperature	Multi tracks and multi layers	Stellite 6	SS8	[51]
Spectrometer	Cavities and cracks in the deposition	-	Inconel 718	Inconel 718	[52, 53]
Spectrometer	Metal powder jet	Single layer	WC, Ni-Fe-B-Si	Fe37-3FN	[54]
Spectrometer	Elemental Composition	Single layer	Multi-	AISI 4140	[55]
Fiber optic spectrometer	Depth of deposition layer	Single layer	Al0.5FeCu0.7NiCoCr	Al5083	[56]
Photodiode	Melt pool width	Single layer	316L	316L	[57]
Acoustic emission sensor	Cracks in the deposition	Multi tracks and multi layers	Ni60A	45	[58]
Acoustic emission sensor	Cracks in the deposition	Multi layers	H13, Ti-6Al-4V	H13	[59, 60]
Acoustic emission sensor	Cracks in the deposition	Multi tracks and multi layers	Multi-	45	[61]
Laser vibrometer optical microphone	Layer cracks and HAZ cracks	Industrial products (valve seats)	Stelite 6	Carbon steel	[62]
X-ray imaging system	Powder flow behavior	-	Ti-6Al-4V	Ti-6Al-4V	[63]
X-ray imaging system	Melt Pool Morphology	Multi-	Ti-6242	Ti-6242	[64]
X-ray imaging system	Temperature, phase transition and stress	Multi layers	Inconel 718	Inconel 718	[65]

Table 3 Comparison among 5 on-line monitoring methods

Monitoring signals	Monitorable objects	Advantages	Limitations	Publications
Image	Morphology and size of melt pool Powder behavior Surface defect	Intuitive process characterization, non-contact measurement	Susceptible to lighting conditions, reflections, plasma arcs, powder flashes, Difficulty in capturing microscopic features	[37, 41, 43]
Temperature	Temperature Thermal history Microstructure (mapping)	High reliability, wide range of applications	Accuracy of different sensors	[32, 45, 50, 66]
Spectra	Elemental composition Powder jet Dimension of a layer	Strong background noise immu- nity, rich physical information at the atomic level	Complex data processing, com- plexity of use and maintenance, limited spectral range	[54, 55, 57, 67]
Acoustic emission	Cracks Pores	Rich information on defects	Low-disturbance environmental conditions	[61, 62]
X-ray	Internal structure Phase transition sequence Powder individual dynamics	Sample penetration, visualizing the evolution of defects	High cost, safety of use	[65, 68, 69]

are increasingly used as DED-LB on-line monitoring signals [70]. Compared to other monitoring signals, image signals can provide non-contact monitoring of morphology, structure, and surface features at high resolution [37]. Commonly used monitoring devices are charge-coupled device (CCD) cameras and complementary metal oxide semiconductor (CMOS) cameras [70]. CCD cameras use a photosensitive element to convert visible light into an electrical signal, which is further converted into a digital image signal by an AD converter; CMOS cameras use each pixel unit on the image sensor and internal integrated circuits to convert the signal, and are more highly integrated than CCD cameras, with lower power consumption and cost, but are usually less sensitive than CCD cameras. There are usually both coaxial and off-axial forms between the camera and the laser beam as shown in Fig. 3 [71]. In this way, diverse morphological and dimensional features at different angles can be obtained.

Coaxial cameras, whose optical axis coincides with the laser beam, are typically used to capture information about the melt pool and its surroundings. Moralejo et al. [72] used a coaxial CMOS camera to monitor the size of the melt pool, and the calibrated. The processed dimensional features were used as control parameters for a feedforward controller to optimize the laser power. Due to thermal accumulation, constant laser power can lead to excessive dilution in the DED-LB process. Hofman et al. [40, 73] explored the correlation between the melt pool width and dilution rate. The melt pool image captured by a CMOS camera was fitted as an ellipse. A feedback control loop was finally realized using melt pool width as a covariate. However, the melt pool is not a standard elliptical shape, Lei et al. [74] used localizing region-based active contours to identify the head and tail of the melt pool. The accuracy of extracting melt pool dimensions was further improved. Colodrón et al.

[37] weighed the accuracy of the sampled images against the processing time. The measurement of melt pool width was implemented based on a field programmable gate array (FPGA). The developed image acquisition and processing system improved the processing speed by nearly 10 times compared to the PC without significantly affecting the performance. Sampson et al. [42] exposed the real edge features of the melt pool by adaptively adjusting the exposure time of the melt pool image captured by a coaxial CMOS camera. Accordingly, a novel edge detection algorithm not based on material emissivity was developed to improve the detection accuracy.

Off-axis cameras allow the melt pool to be viewed from the side or from other angles, providing more comprehensive dynamic information. However, off-axis monocular cameras suffer from a blind spot in the field of view, which is inevitably obscured by the already formed track [47]. Hsu et al. [38] used a trinocular CCD camera to capture the calibration bar and the deposition boundary from an overhead angle. The melt pool height was calculated based on the known distance of the laser head from the substrate. A deviation of only 2.3% was obtained. In addition, the calibration bar technique was utilized to compensate for field-of-view (FOV) effects and see-through phenomena, resulting in a significant cost reduction. It is worth noting that the use of multi-ocular cameras, while giving a variety of viewing angles and 3D reproduction results, makes it difficult to ensure that each camera is mounted at exactly the same angle, distance, and focal length. Based on a triangulation method, Donadello et al. [75] implemented melt pool height measurement on an original coaxial device. Although the system is not as sensitive as a multi-camera, it was shown to be able to be used in closed-loop feedback controllers at the sub-millimeter level. Sun et al. [71] used a coaxial device similar to [75].

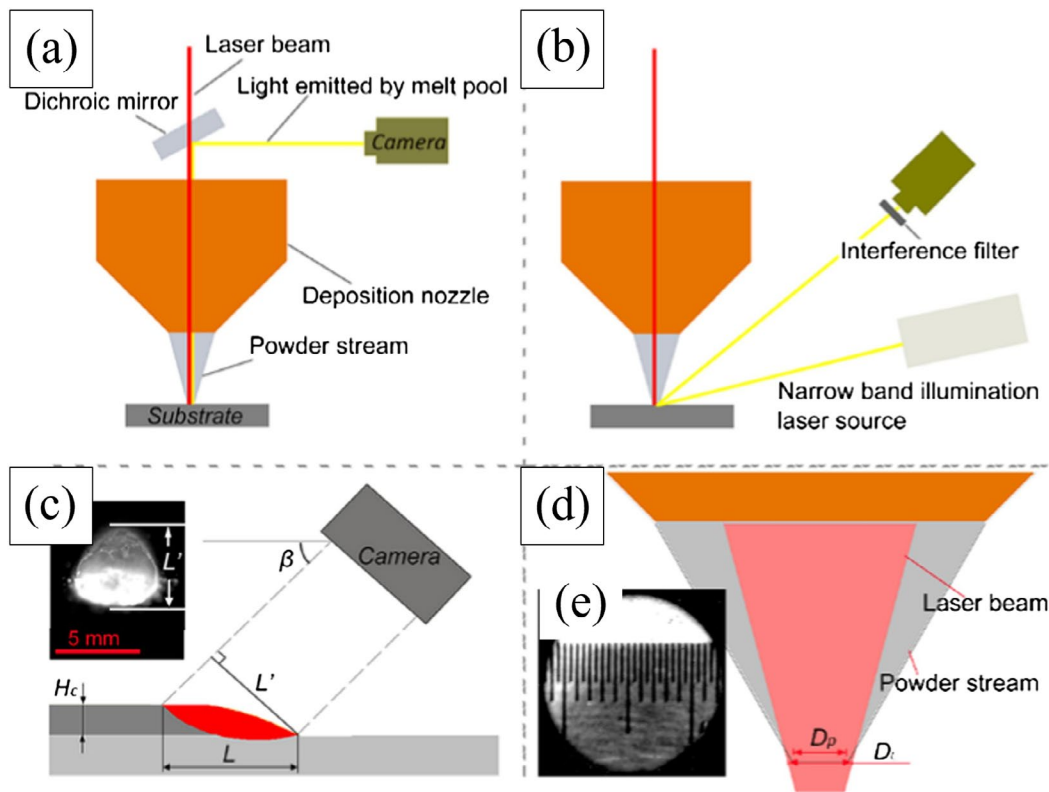


Fig. 3 Schematic setup of the imaging system; (a) coaxial camera installation; (b) off-axial camera installation; (c) melt pool morphology observed using off-axial imaging system; (d) illustration of laser

beam and powder stream at processing area; (e) size of vision area through powder feeding nozzle [71]

Based on the measured melt pool width, two curve fitting methods, parabolic and arc, were utilized to predict the melt pool height in real time, achieving a prediction accuracy of 92%. In addition to height measurements, Smurov et al. [39] recorded the flight trajectory of each powder particle by means of a CCD camera. The particle flux was found to form a conical volume at an angle of about 18° with respect to the substrate normal. The effect of the carrier gas flow rate on the particle flight velocity was also thus analyzed, which is important for optimizing the powder feeding conditions.

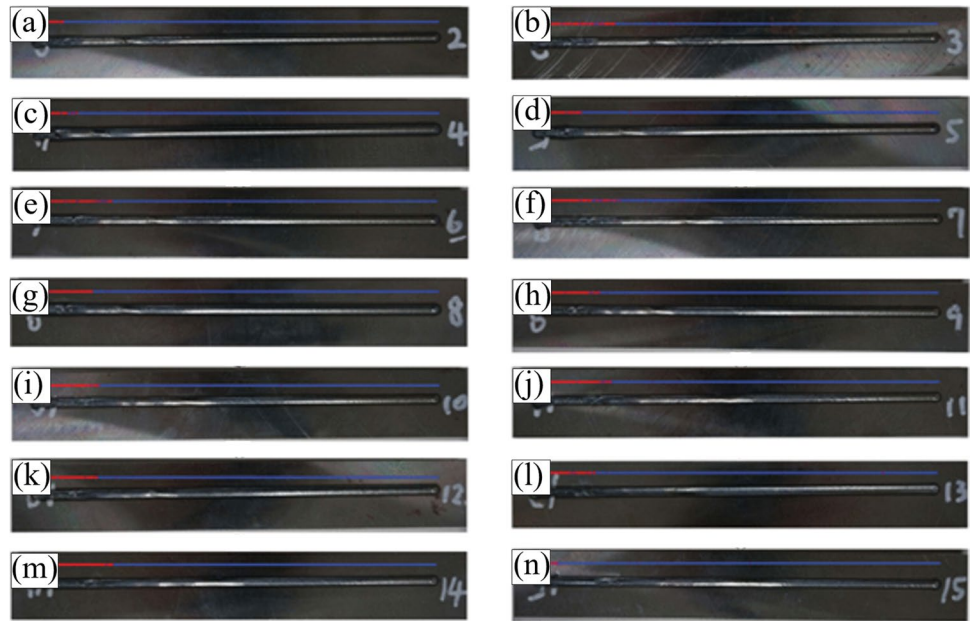
All of these on-line monitoring means based on image signals are subjected to similar processing steps, such as the necessary image filtering, threshold segmentation, and edge detection and feature extraction of the melt pool image [36, 47, 74], which increases the human interference in the image processing. Fuzzy thresholding, multi-scale morphological operators, and adaptive algorithms have been applied to the DED-LB process to improve the melt pool contour extraction accuracy and system stability [42, 76, 77]. However, the adaptive ability in the face of complex scenarios is still limited. In addition, due to the complexity of the DED-LB process, a good quality of deposition can never be judged by observing a single melt pool feature. In contrast, machine learning is characterized by automatic feature learning and stronger generalization ability.

Kao et al. [78] found that there was no significant difference between the melt pool images of low and normal quality processes and used a machine learning approach for on-line prediction of the quality of the deposition. Experimentally, it was found that convolutional neural network (CNN) outperformed autoencoder in feature extraction and classification, which was mainly due to the advantages of its hierarchical feature learning and depth-based structure. The acquired coaxial image was taken as input and after multiple convolutional, pooling, and fully connected layers, the output was the width, height, and the ratio of the height of the heat-affected zone to the height of the deposition layer. The judgment results by CNN under different process parameters are shown in Fig. 4. Red color indicates poor processing and blue color indicates normal processing, both of which have accuracy rates higher than 95%. However, the implementation of deep learning model requires a large number of training datasets, which often requires a lot of effort to obtain [79].

2.2 Monitoring methods based on temperature signals

When a high-energy laser beam irradiates the surface of the substrate material, it is absorbed and converted into thermal

Fig. 4 Judgment results of the deposition process. **a** 750 W and 300 mm/min. **b** 750 W and 450 mm/min. **c** 750 W and 600 mm/min. **d** 1000 W and 300 mm/min. **e** 1000 W and 450 mm/min. **f** 1000 W and 600 mm/min. **g** 1000 W and 750 mm/min. **h** 1250 W and 450 mm/min. **i** 1250 W and 600 mm/min. **j** 1250 W and 750 mm/min. **k** 1250 W and 900 mm/min. **l** 1500 W and 600 mm/min. **m** 1500 W and 750 mm/min. **n** 1500 W and 900 mm/min [78]

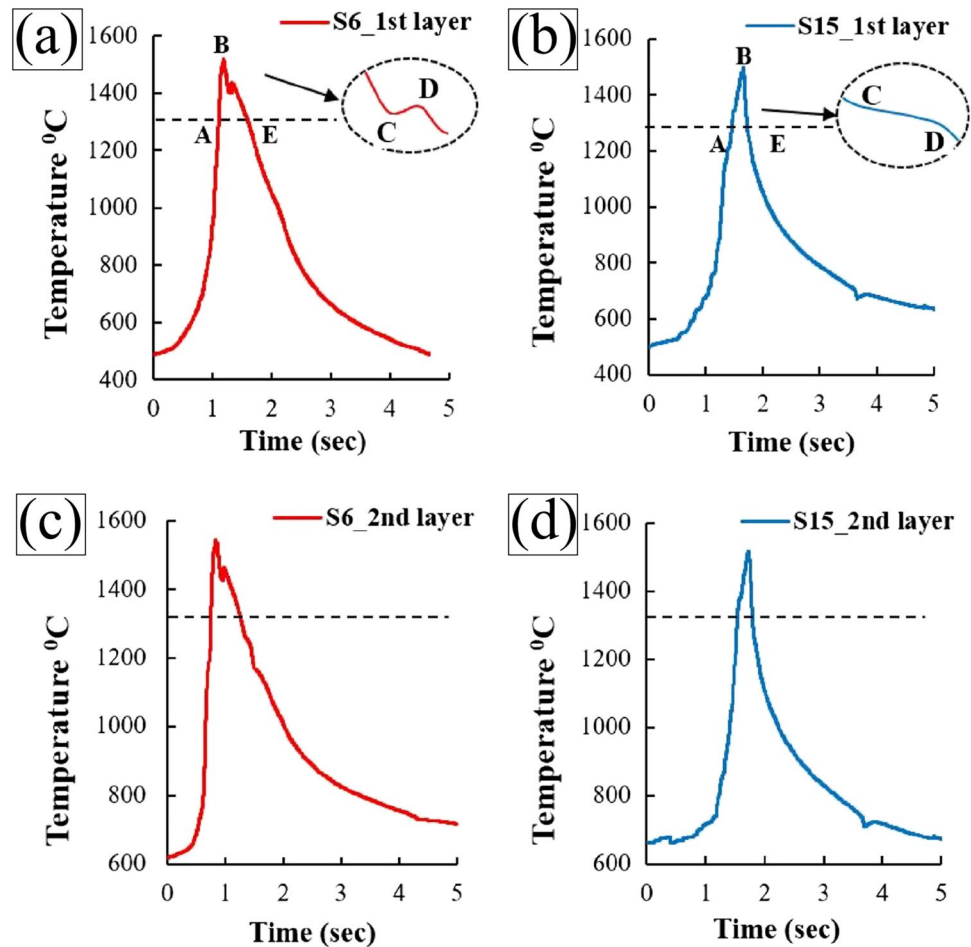


energy. The substrate surface and the powder are heated by the heat source and a melt pool is formed in a localized area centered on the point of laser beam irradiation [67]. With the movement of the laser beam, the melt pool is rapidly cooled and solidified [56]. Change in temperature during this process is also accompanied by changes in microstructure and organization [52, 80]. Bi et al. [57] verified the dependence of the temperature signal on the main process parameters, including laser power, powder feed rate, and scanning speed. The results showed good correlation of dilution and size with the temperature signal. It can be seen that the temperature distribution in the process zone and its transient behavior directly reflects the powder-matrix bonding and greatly affects the part properties [81]. It is particularly important to monitor the temperature field using temperature sensing devices. Temperature monitoring devices are categorized into contact and non-contact measurements according to their mode of operation. Due to the limitation of temperature measurement range and response speed [82], contact temperature sensors such as thermocouples are not suitable for temperature monitoring of melt pool with high temperature, large temperature gradient, and fast cooling rate. However, the use of multiple thermocouples to measure the temperature of the substrate is a good choice [83, 84]. Non-contact pyrometers [39, 81] all measure temperature based on the principle of infrared radiation. These include single-spot pyrometers that can measure the temperature at a single point of the melt pool, multi-wavelength pyrometers that are capable of eliminating some of the effects of surface reflection and scattering, and infrared thermography that allows direct access to the temperature distribution on the surface of the melt pool [54]. It is shown in Table 1 the different types

of a model of thermometer performance parameters, only as a reference comparison. Appropriate sensing equipment should be selected depending on the monitoring object and specific needs.

Thawari et al. [84] monitored the temperature and deflection variations of substrates with different fixation methods using type K thermocouple and laser displacement sensor. A combination of simulation and experimentation was carried out. The results showed that simple and fixed supports produced 40–50% less deflection than cantilevers. In all samples, multi layers produced less deflection than single layers. This is precisely because the change in temperature gradient allows the material to expand and contract at different rates. Temperature not only causes deformation but also microstructural changes. In a subsequent study, multiple thermocouples were used to monitor the thermal history [83]. It was found that the addition of Inconel 625 reduced the temperature by 20–22% compared to direct deposition of Stellite 6. Fine microstructures and crack-free tracks were formed. However, validation of the mechanical properties of the deposition layers was lacking. In a multi-layer deposition experiment involving Stellite 6 and Inconel 718, Thawari et al. [32] measured the melt pool temperature graph shown in Fig. 5. It is shown that the melt pool thermal history trends are similar regardless of the deposition material. In addition, it was observed that the melt pool temperature in the second deposition layer was higher than that in the first layer, such temperature increase was attributed to the accumulation of heat between the layers for a short period of time. As a result, if the substrate can be preheated before the start of the deposition, the thermal gradient can be effectively reduced and the deposition performance can

Fig. 5 Melt pool temperature plot for S6 and S15. **a** Stellite 6 (1st layer), **(b)** Inconel 718 (1st layer), **(c)** Stellite 6 (2nd layer), and **(d)** Inconel 718 (2nd layer) [32]



be improved. Srisungsitthisunti et al. [85] obtained similar conclusion when conducting experiments on the deposition of multi layers with Inconel 625 powder.

In order to investigate the variation of thermal cycling with process parameters and its effect on the mechanical properties of the deposition layer, Muvvala et al. [86] recorded the thermal cycling of the DED-LB process with a single-spot, monochromatic pyrometer and estimated the heating and cooling rates. The scanning speed was found to have a greater effect on the cooling rate than the laser power. The resulting conclusion was used in the DED-LB experiments of the composite of Inconel 718 and TiC. The melt pool thermal cycling was monitored using a single-spot monochromatic infrared thermometer at scanning speed of 400 mm/min and 1200 mm/min, respectively. Figure 6 [41] demonstrates the decomposition of TiC during solidification to form a dendritic structure during slower cooling, when the melt pool lifetime is too long and exhibits brittleness and poor wear properties. The melt pool lifetime that produces good orbital quality is in the range of $0.25 \text{ s} < \tau \leq 0.45 \text{ s}$, which only applies to specific materials [33]. In addition, Muvvala et al. [43] explored the effect of different waveform lasers on the

melt pool lifetime by recording the thermal history of the melt pool for modulated power signals with different duty cycles. The melt pool temperature was found to oscillate around the melting point at a duty cycle of 40%, which accelerated the cooling rate and refined the TiC particle coating. Srisungsitthisunti et al. [85] tested the cooling rate of the melt pool at different laser powers. Lower laser powers produced faster cooling rates, leading to smaller grain sizes and higher microhardness. In addition to monitoring melt pool thermal history, infrared cameras can provide more detailed spatial and temporal signals than pyrometers, but the calibration process requires defining material emissivity that changes at higher temperatures [53]. Doubenskaia et al. [87] used infrared thermography to measure the melt pool brightness temperature. The true temperature distribution in the region of the deposited layer was obtained using the gray body assumption at different process parameters as shown in Fig. 7. The emissivity and the orbit size during the phase transition were further determined from the liquid-solid phase transition point of the material. As can be seen from the figure, an increase in track width and the size of heat-affected zone (HAZ) is evident with increasing laser power.

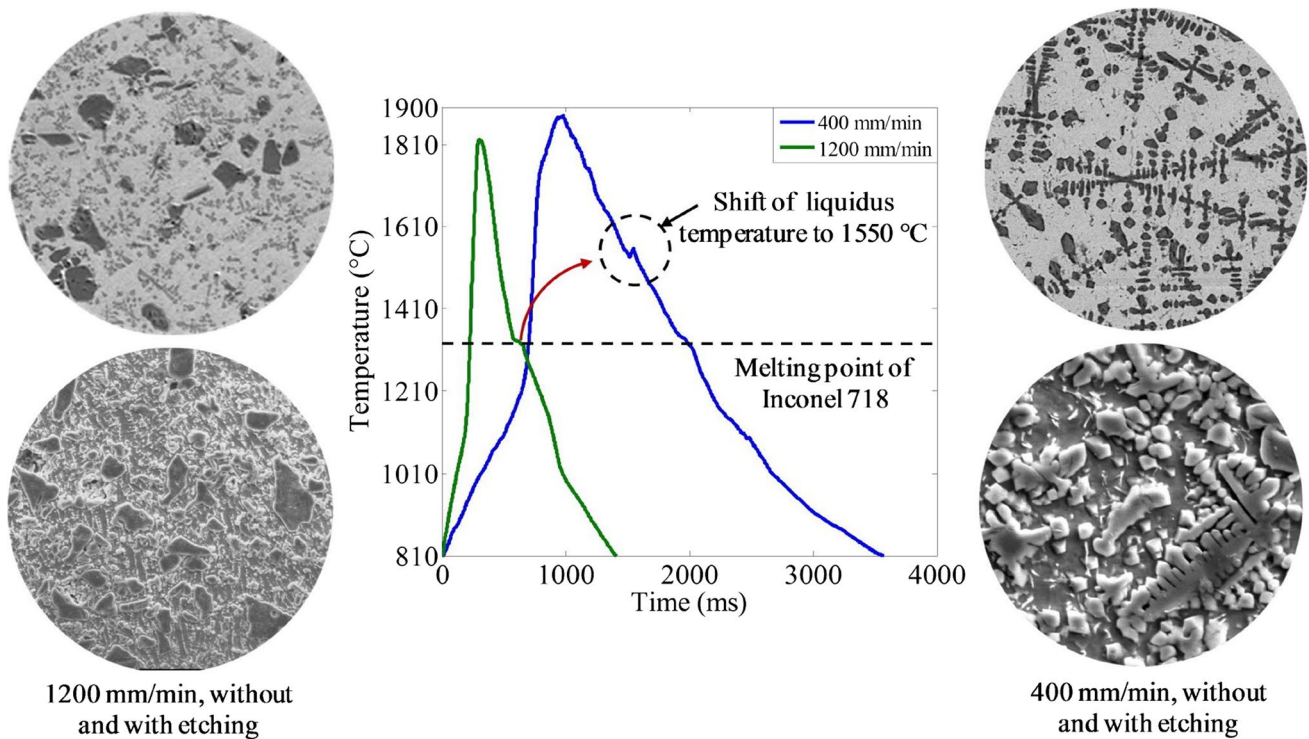


Fig. 6 Relation between slope of solidification shelf and microstructure [41]

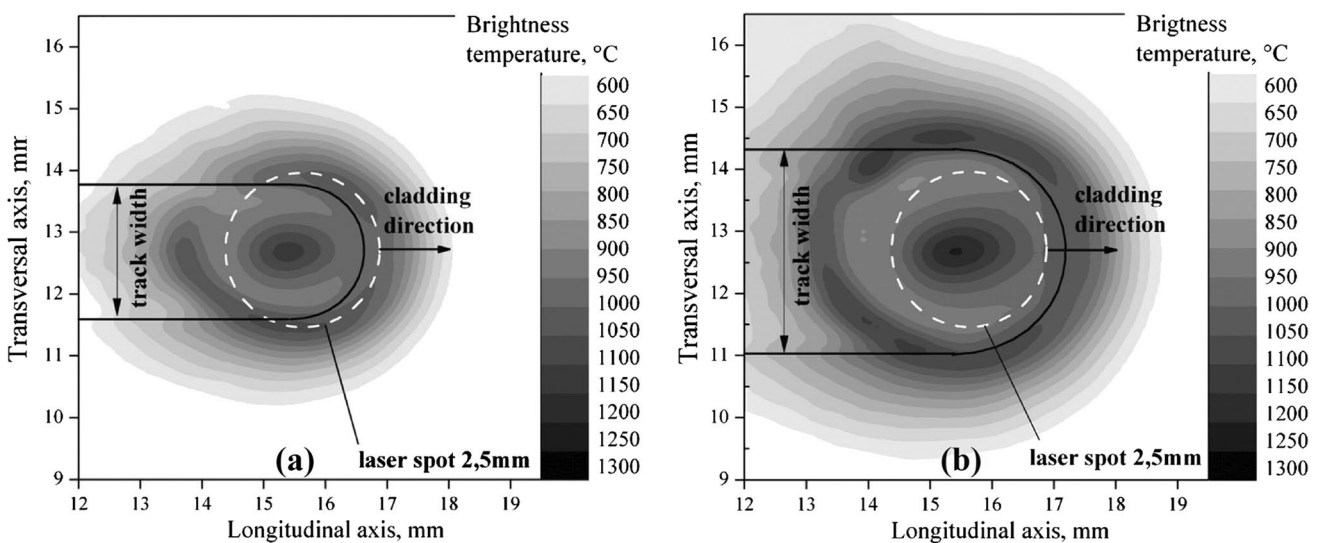


Fig. 7 Brightness temperature distribution in the clad zone obtained by calibration of infrared camera with the black body. Scanning speed $S=1$ mm/s, laser spot size $d=2.5$ mm, and powder feeding rate $F=10.5$ g/min. **a** $P=500$ W, $f=6$ L/min and **(b)** $P=750$ W, $f=9$ L/min [87]

The pyrometer, although capable of providing temperature distribution and thermal history information at a higher response rate than a camera, is unable to visually characterize internal defects and cannot be used as a single-factor characterization information of the deposition performance. Single-input-single-output (SISO) control systems with only

temperature as the output variable have been shown to be unable to guarantee uniform and consistent track morphology when controlling multi layers of deposition [88, 89]. This is due to the fact that different melt pool morphologies may have the same temperature, which depends on the dynamic balance of heat input and heat loss. To address

this issue, Tang et al. [90] and Song et al. [34, 35] developed a layer-to-layer control system and a camera temperature-based multi-source hybrid control system, respectively, which could effectively improve the dimensional accuracy of parts. Although cameras can provide visual process information, image acquisition is affected by ambient lighting conditions, reflections, plasma arcs, powder flash, and other noises [38, 55]. Taken together, the temperature signal is often used as an auxiliary signal to strongly complement the interferometric visible light signal in practical engineering applications. For example, Xu et al. [36] constructed a multi-source image monitoring system based on the combination of infrared thermography and high-speed camera. Six complementary features of melt pool and splash were extracted from the infrared thermal camera and high-speed camera, respectively, and a classification accuracy of 99.5% of fine features was realized.

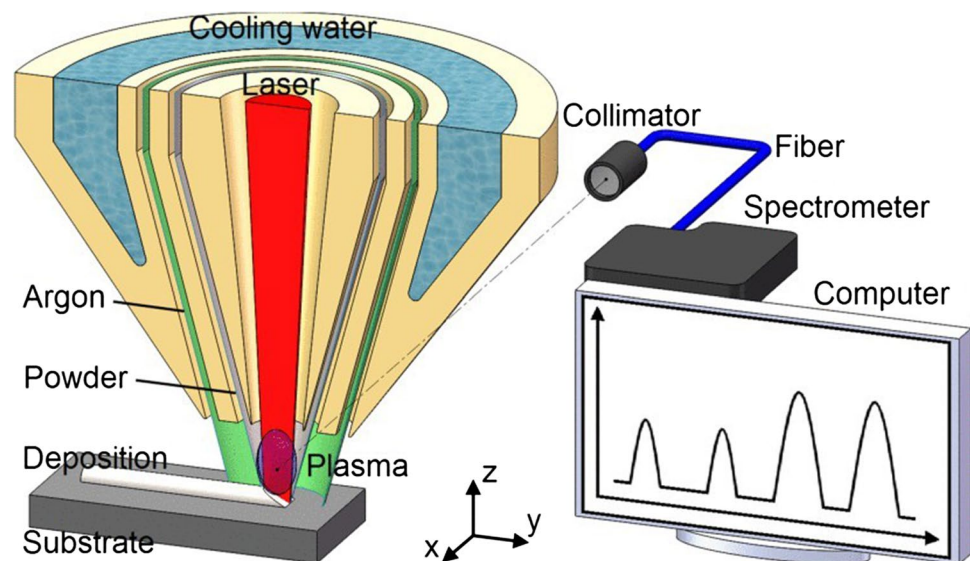
2.3 Monitoring methods based on plasma spectral signals

Fundamentally, the on-line monitoring methods described above are closely related to optical signals. Typically, images captured by cameras are performed based on visible light signals, whereas temperature measurement devices such as pyrometers and thermal imaging cameras are based on thermal radiation from infrared light to obtain temperature information [91]. A special spectral intensity signal, plasma spectroscopy, can also be used for on-line monitoring and diagnostics during DED-LB [92]. A schematic of laser-induced plasma detection is shown in Fig. 8 [92]. With the help of plasma spectral information, it is possible to observe the atomic or ionic features produced by pulsed laser ablation of the sample during DED-LB in the frequency domain

of a specific wavelength range. Spectral signals have stronger background noise immunity than image and temperature signals [93]. In addition, it is able to provide richer physical information at the atomic level [46]. Spectral analysis involves complex data processing techniques and equipment that are costly to use and maintain. Commonly used spectral sensing and analysis equipment includes photodiodes and spectrometers. Photodiodes have a high response speed, but only detect the intensity of the light signal and do not provide detailed information about the spectral distribution. Spectrometers can measure light signals at multiple wavelengths simultaneously, providing detailed elemental composition of materials through spectral characterization. Furthermore, many researchers have obtained information such as plasma or electron temperatures, spectral intensities, and spectral line intensity ratios from the plasma plume during DED-LB [94, 95] to characterize the changes in microstructural and mechanical properties, the generation of defects such as pores and cracks [93, 96]. The correlation between process parameters and plasma spectral information is also explained [94].

Photodiodes are generally used to monitor the overall intensity of a spectrum without being able to distinguish between the different wavelengths of the light components of the spectrum. Miyagi et al. [97] used three photodiodes integrated in a laser head to monitor the signal intensities of thermal radiation, plume emission, and laser reflection from the melt pool. The specific spectral signals were received through selective filters of different wavelengths. The variations of different signal intensities with respect to process parameters and the relationship between deposition layer size and signal intensity were obtained by setting different combinations of process parameters. The experimental results showed a good correlation between the thermal

Fig. 8 Schematic diagram of the detection of laser-induced plasma [92]



radiation signal intensity, melt pool width, and laser power, from which a feedback control system for thermal radiation in the melt pool was established. In addition to being able to characterize the melt pool dimensions, Lin et al. [58] and Bi et al. [12, 57] used photodiodes to monitor the

thermal radiation energy and correlate it with the temperature, respectively. Photodiodes are favored in control systems that do not require access to elemental composition due to their simple installation and fast response.

Laser-induced breakdown spectroscopy (LIBS) is currently the most commonly used technique for acquiring plasma plumes and quantitatively analyzing the target in terms of elements, which is characterized by on-line analysis and non-contact work [59, 60, 98]. It can be adapted to the extreme working conditions of DED-LB processes. Lednev et al. [96] developed a LIBS probe [99] and performed in situ monitoring and quantitative analysis of melt pools. As shown in Fig. 9, the LIBS signals of atomic (Fe I 278.81 nm) and ionic (Fe II 274.67 nm) ferrous wires in the defective deposition have a greater average intensity compared to the optimal deposition, and this difference has a significance level of 95%. However, obtaining LIBS spectra with good signal-to-noise ratio places high demands on the sampling and analyzing rates of the sensor and spectrometer. During the DED-LB of high entropy alloy (HEA) powder with aluminum substrate, Ni et al. [94] obtained plasma emission spectra in the wavelength range of 400–850 nm at different scanning speeds. Figure 10 shows the variation of Al-II spectral intensity versus layer depth at different scanning speeds. It can be seen that the spectral intensity of Al-II decreases with the increase of scanning speed. The trend of the depth of deposition layer with scanning speed is basically comparable with the spectral intensity of Al-II. Consequently, to a certain extent, the spectral intensity of Al-II can characterize the change of the depth of the deposition layer. Compared to LIBS sampling in the melt pool, Sdvizhen-skii et al. [98] changed the monitoring object to a metal powder jet, which would not be disturbed by the blackbody

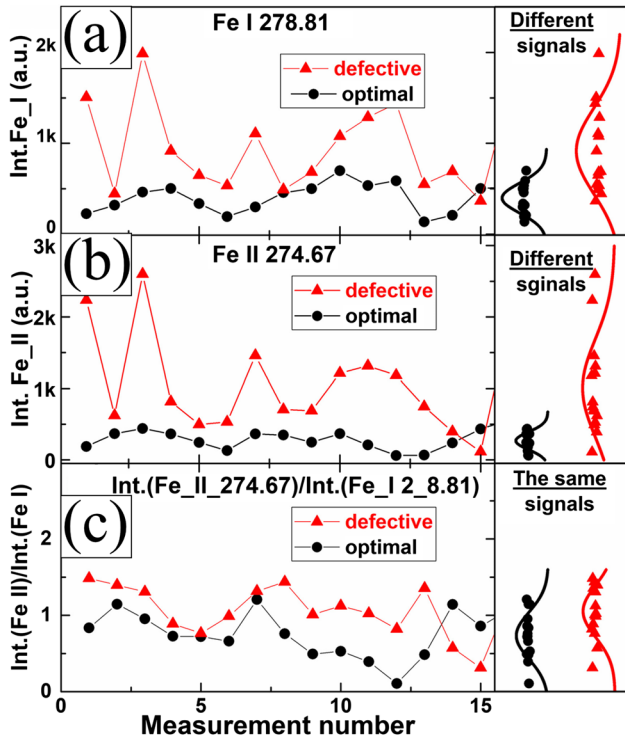


Fig. 9 Shot-to-shot LIBS signals comparison for in situ ablation of the melt pool during optimal (black color) and defective (red color) laser welding: (a) atomic iron line Fe I 278.81 nm integral; (b) ionic iron line Fe II 274.67 nm integral; (c) ionic to atomic iron line integrals ratio (Fe II 274.67 / Fe I 278.81) [96]

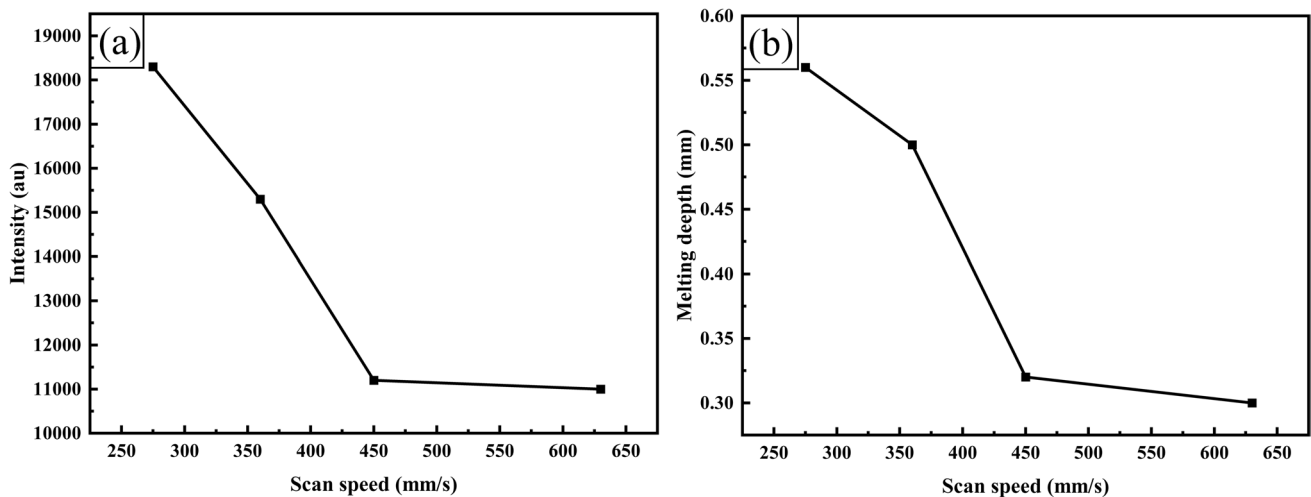


Fig. 10 The influence of scanning speeds on layer depth and spectral intensity [94]

radiation of the melt pool and the reflection of the laser beam. This led to a higher robustness. However, due to the inhomogeneous distribution of particle density, the LIBS sampling points need to be continuously optimized by 2D mapping. Optical emission spectroscopy (OES) is an alternative plasma spectroscopy analysis technique to LIBS. It has a much higher spectral resolution to the point of being able to analyze subtle changes in material composition at greater depths [95, 100]. However, OES usually brings more data volume, which inevitably adds difficulties to the extraction and categorization of valid information [62].

The DED-LB process undergoes solid-liquid-gas phase changes [101]. The plasma characteristics captured by the spectrometer above the melt pool differ from the elemental characteristics in the melt pool due to the effect of saturated vapor pressure. In order to compensate for the compositional deviation due to the partial pressure of the metal gas, Wang et al. [102] measured the elemental weight% of the deposition layer using energy-dispersive spectroscopy (EDS), from which calibration curves for the intensity ratio between spectral lines were established and a monitoring system was constructed for application to the DED-LB process. When the alloy vapor concentration above the melt pool was greater than 3%, the relative deviation of the components was less than 8%. A component concentration of less than 3% significantly affected the error rate in the spectra. Such results imply that the monitoring system needs further improvement. Song et al. [92] trained support vector regression (SVR) models for predicting elemental concentrations using spectral intensity ratio, spectral intensity ratio, and spectral integral dual features, respectively. In order to validate its effectiveness, prediction comparison experiments were conducted with the calibration curve method at different nominal elemental concentrations. The results shown in Fig. 11 indicate that the SVR method can effectively solve the nonlinearity problem of the calibration curve in the low concentration region. In addition, SVR2 with line intensity ratio and integral intensity as inputs has a higher feature dimension and achieves better prediction results than SVR1 with line intensity ratio alone. This demonstrates that high-dimensional features can better capture the relationship with elemental compositions. In addition to calibration issues, the low laser energy density used by Wang et al. [102] was unable to observe spectral lines emitted by refractory elements such as W and Mo during depositing nickel-based high-temperature alloy powders. De Baere et al. [61] did not find plasma information features when measuring radiation spectra in the range of 400–850 nm. The inability to generate plasma plumes at lower laser energy density was confirmed experimentally, which limits the application of plasma spectroscopy in on-line monitoring techniques for DED-LB.

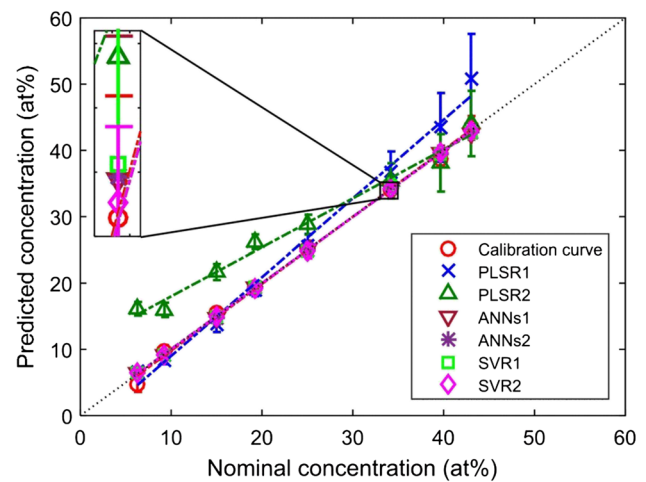


Fig. 11 Predicted Al concentration and nominal Al concentration using calibration curve, PLSR, ANNs, and SVR methods [92]

2.4 Monitoring methods based on acoustic emission signals

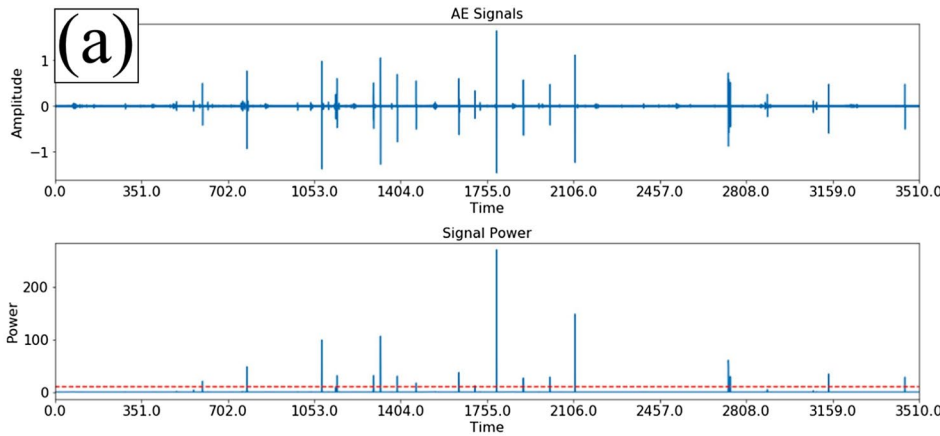
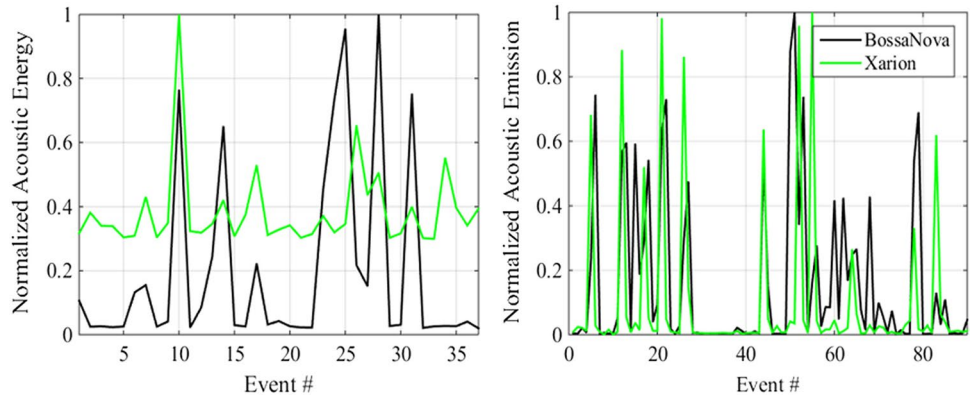
Acoustic emission (AE) is used to obtain information about the interior of a material based on the detection of tiny acoustic wave signals released by the material under stress, temperature, pressure [63, 103, 104], etc. During the DED-LB process, the complex physicochemical processes arising from the interaction of the high-energy laser with the material are accompanied. A series of acoustic vibrations are induced, resulting in an acoustic emission signal. This contains a wealth of information related to cracks, pores, and other defects [50, 51, 105]. However, the AE signals are weak and need to be collected and analyzed with the help of highly sensitive instruments. AE signal acquisition devices can be categorized into contact [106] and non-contact types [66] according to the sensor mounting position. Contact sensors are generally less expensive and allow direct contact with the object to be measured for the most intuitive measurement results. Nevertheless, few contact sensors are able to adapt to the high temperature of the DED-LB process. Cooling methods that incorporate waveguide rods or water circulation are usually required. Among other things, waveguides can also act as a medium for the propagation of certain wave modes [105, 107]. Non-contact sensors are capable of non-destructive testing, but place high demands on cost and environmental conditions.

Garcia De La Yedra et al. [66] used a laser vibrometer and an optical microphone to monitor layer cracking caused by thermal stress and HAZ cracking acoustic waves, respectively. The sensitivity was mutually verified by normalized acoustic energy images under different samples shown in Fig. 12, providing a more reliable crack analysis. Based on the phenomenon that the generation of cracks or defects

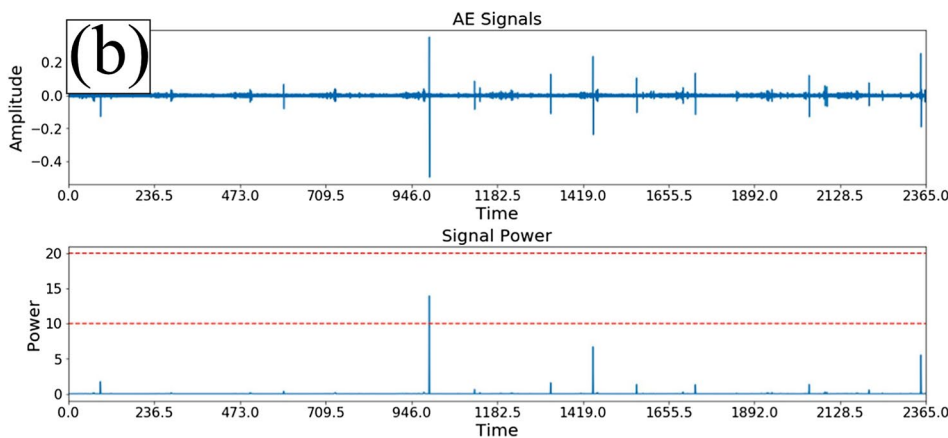
during the deposition process tends to emit energy shocks, Li et al. [105] utilized an AE sensor to collect the AE signals and signal energy during the deposition process in real time, as shown in Fig. 13. It can be found that the AE signals of

the normal deposition process are relatively flat, while the amplitude of the signal energy at the cracks is much larger than the normal state. Wang et al. [108] used AE technique combined with finite element analysis to investigate the

Fig. 12 Normalized acoustic energy per acoustic emission event monitored by an optical microphone (green) and a laser vibrometer (black) for both samples [66]



The AE signal of the cladding process with cracks



AE signal of the cladding process without cracks

Fig. 13 AE signal and real-time signal energy in the deposition process (the real picture on the right is the coloring development detection effect of the deposition layer, and the cracks will appear as red tracks) [105]

location of crack generation and the temperature range of crack expansion during DED-LB. The results showed that the number of cracks in the DED-LB process was positively correlated with the coating area and thickness as well as the cooling rate. Strantz et al. [109] utilized AE to monitor the crack extension process during DED-LB. A link between the AE parameters and the location of crack generation was established. Gaja et al. [50, 51] collected AE signals from a mixed-metal powder deposition process and successfully differentiated between pore and crack features by using K-Means clustering method, logistic regression (LR) model, and neural network (ANN) model, respectively. The AE signals generated by pores were found to have a short decay time and small amplitude. The AE signals triggered by cracks were found to have short duration and high amplitude. Taheri et al. [106] defined five states of the DED-LB process by monitoring the AE signals of the substrate using a clustering algorithm similar to that in [51]. These analyses revealed that the AE monitoring technique has great potential for on-line monitoring and defect diagnosis of DED-LB process. Parameters such as signal amplitude, duration, and rise time are key features for identifying the source mechanism of defects and the severity of defects.

In addition to studies on the relationship between AE signals and the type of defects in the process, the effect of different processing conditions on the characterization of AE signals has been explored by an increasing number of scholars. Li et al. [105] obtained characteristic parameter datasets of normal deposition and suspected crack signals by changing a certain process parameter. And a network model named SRCD for deposition layer state identification and crack defect detection was constructed, as shown

in Fig. 14. The constructed deep learning model was able to effectively recognize 11 crack-generating situations caused by the abnormality of a certain process parameter, and the accuracy of the model was 99.76%. Based on the t-SNE algorithm for feature optimization, Li et al. [110] extracted the time-domain features (e.g., root-mean-square value, kurtosis, sparsity factor, and sample entropy) and frequency-domain features (e.g., energy entropy) of the AE signals under three sets of different process parameters. The results obtained 92.8%, 89.0%, and 91.8% accuracy respectively. Whiting et al. [107] developed a powder mass flow monitoring system based on AE signals by integrating a non-contact AE sensor into the powder feed line. The AE system was tested to produce a signal proportional to the mass flow rate with a correlation coefficient of 0.985 between the two signal samples. In summary, the AE characteristics in DED-LB can effectively analyze the processing state of substrates. AE signals generated by melt pool vibration, powder injection, and material deformation under different process parameters can effectively characterize the processing state and quality. The utilization of this method for troubleshooting of deposition layers or more complex parts is a hot research topic in the future.

2.5 Monitoring methods based on X-ray signals

The four on-line monitoring signals mentioned above are the most commonly used sensing signals in DED-LB processes today, but have limited ability to characterize process information. More advanced monitoring equipment should be used. In situ X-ray imaging has proven to be a very effective technique. When a polychromatic X-ray beam irradiates and

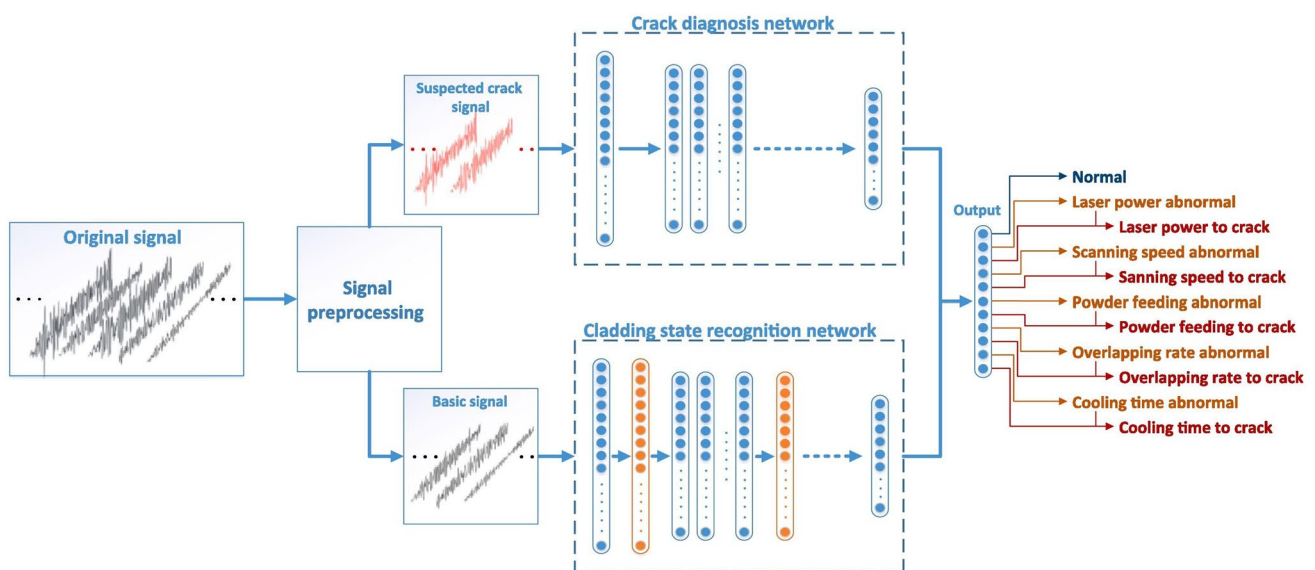


Fig. 14 The model of SRCD's framework presented in this paper [105]

penetrates the sample, a scintillator converts the X-ray beam into visible light and an imaging display by a high-speed camera. Further information on the internal structure of the material and defect generation can be obtained [48]. X-ray imaging has been progressively matured for on-line monitoring of powder bed fusion (PBF) [64, 68, 69]. Drawing on this, several researchers have recently conducted similar studies in DED-LB in order to shed more light on the kinetic interactions between the laser, the powder, and the melt pool.

In order to reveal the effect of powder flow on melt pool fluctuations and on porosity, Wolff et al. [48, 65] set up two DED systems with different orders of magnitude of powder flow rates and monitored them separately by X-ray imaging. The small system with low powder flow rates showed lock holes similar to the PBF experiments, while the large system with industrial scale showed more fluctuations concentrated on the surface of the melt pool. A sequence of images under X-ray imaging is shown in Fig. 15, where the red dashed circles in the top row indicate powder with pores captured on the melt pool surface, and the yellow dashed circles in the bottom row indicate the escape path of the holes. In the subsequent work, high-speed X-ray imaging was used to capture, visualize, and classify the pore-generating process [111] as a means of elucidating the formation mechanism to better guide practical production and applications. Based on an edge image template combined with a Bayesian inference approach, Lindenmeyer et al. [49] used X-ray imaging for the first time to automatically extract melt pool shape and size. The proposed method alleviates the bottleneck of manually analyzing tedious data, but the detection accuracy is still greatly affected by noise. Chen et al. [44] used synchrotron X-ray imaging to investigate the effects of process conditions such as laser power, powder feeding rate, and scanning speed on melt pool morphology during Ti-6242 deposition. In addition, the processes of powder sintering

and pore formation were similarly observed. Chen et al. [45] quantified key features and guided the diffraction process through X-ray imaging. The melt pool temperature gradient was isolated and the phase transition sequence and stress state of the deposition process were obtained.

X-ray imaging is an important visualization tool for capturing melt pool kinetics and defect evolution. In addition, X-ray diffraction and small angle X-ray scattering (SAXS) are also analytical techniques related to X-ray signals, which are used to monitor solidification kinetics and precipitation evolution, respectively [112]. The current X-ray signals have been gradually applied in on-line monitoring of DED-LB. However, due to the complexity of the related equipment and the strong radiation of X-rays, specific DED-LB system needs to be designed. The on-line monitoring technology of DED-LB based on X-ray signals still has some limitations at present, but it has a good potential for development. Therefore, the research and optimization of X-ray imaging technology will help to deeply understand the DED-LB process and promote the further application and development of DED-LB.

3 Control strategies for DED-LB

DED-LB, as a complex process, is still under open-loop control in current production. The combination of process parameters usually needs to be adjusted and optimized through multiple experiments and analyses. However, DED-LB involves the integration of multiple physical fields. The optimal level of each process parameter also depends on the material, working conditions, and real-time interaction of multiple parameters [105]. Offline process parameter optimization does not adequately capture the severe impact of complex time-varying features on process stability. It is also insufficient to overcome the geometrical deviations and

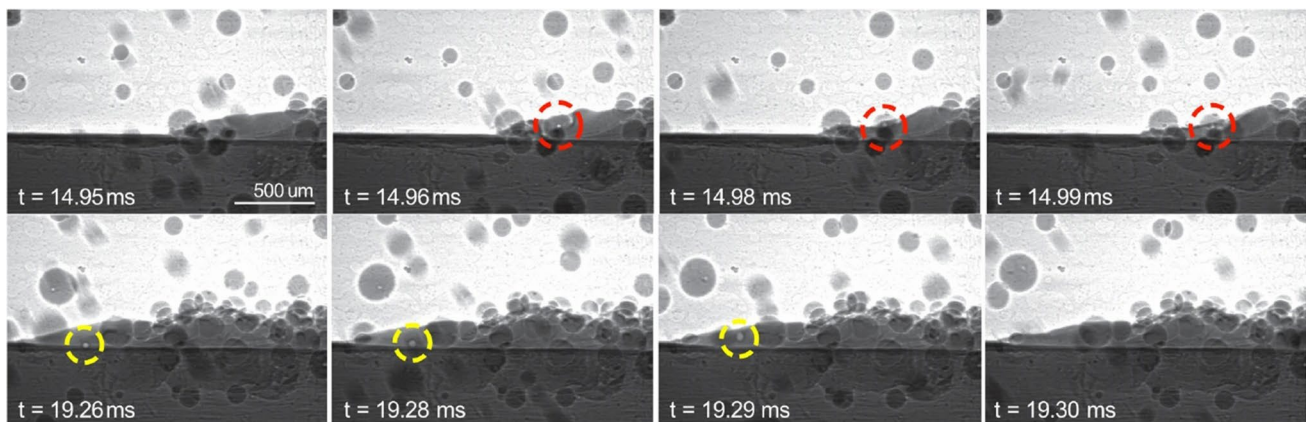


Fig. 15 Sequence of X-ray images from large-scale DED with laser power 200 W, scan speed 100 mm/s, and powder flow rate 535 mg/s [48]

distortions of the part due to continuous thermal build-up. To realize real-time control of the DED-LB process, many scholars have carried out related researches. Different sensing devices have been used to capture monitoring signals, such as images, temperature, spectra, AE, and X-rays to characterize the information in the DED-LB process. Thereby, the closed-loop control system has been established. By timely adjusting the process parameters, the coating quality can be effectively improved, the defect rate can be reduced [24, 113, 114], and the automation and intelligence of DED-LB process can be realized.

This section will focus on the different control strategies of DED-LB quality control system, including specific control methods, optimization algorithms, and evaluation indexes of deposition performance. The input control signals described in this section are all based on the on-line monitoring signals described in Section 2. The aim is to explore the three-dimensional mapping relationships among process parameters, on-line monitoring signals and deposition quality.

3.1 Conventional control methods

Classical PID control, fuzzy control, feedback control, feedforward control, and model predictive control (MPC) are included within the conventional control methods. The transient processes of DED-LB constructed based on the physical principles such as mass balance, energy balance, momentum balance, heat conduction equation, and heat convection equations [115, 116] or model transfer methods [117] are referred to as mathematical analytical model, which can be used to accurately represent the control system behavior. However, considering the complexity of the DED-LB process, there exists a nonlinear relationship between the controller input and output control variables [118]; empirical models fitted on the basis of experimental data are the most frequently used. Conventional control methods, based on simple control logic, achieve quality control of DED-LB through feedback mechanisms. The stability and effectiveness of these methods have been thoroughly validated in numerous studies and practical applications.

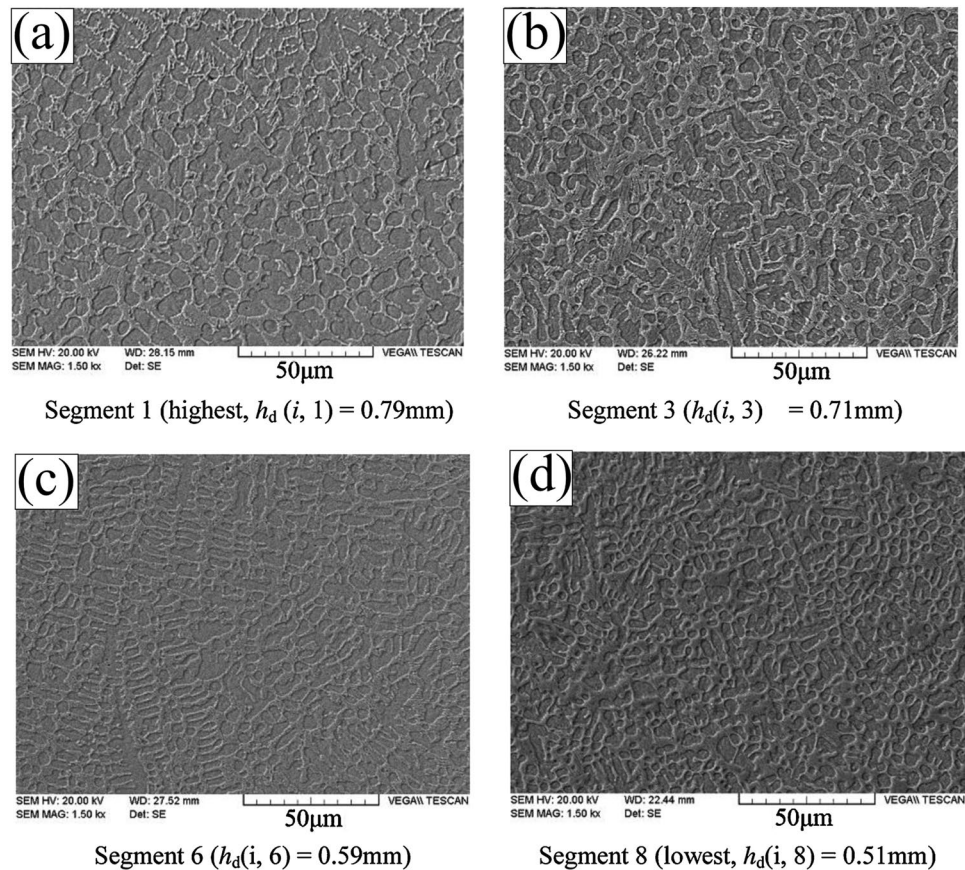
The geometrical characteristics of the melt pool are the most effective control parameters. Hofman et al. [40, 73] developed a CMOS camera-based DED-LB control system capable of regulating the laser power in real time. This closed-loop system was able to compensate for heat accumulation during the deposition process within 1 s to obtain a customized melt pool width and a stable dilution rate. Similarly, Akbari et al. [119] selected laser power and melt pool width as control input and output variables, respectively, and verified the controller performance with more diverse metrics based on [40]. Moralejo et al. [72] and Ding et al. [120] designed a feedforward-feedback controller by

combining the characteristics of conventional PID controller's and feedforward controller, respectively. This combined control approach could improve the response speed and control accuracy of the system. The feedforward controller could adjust the DED-LB power in advance according to the desired DED-LB width, thereby reducing the response time of the system. Meanwhile, the PI controller could make feedback adjustment according to the actual melt pool width to keep the deposition layer width near the desired value. Fathi et al. [121] also proposed a similar feedforward PID controller, selecting scanning speed as input control variable and melt pool height as output. The performance of this controller has been well validated in curved surface part fabrication. When facing the same surface manufacturing challenge, Shi et al. [122] developed a height-memory strategy and used multiple PI controllers to segmentally control of unequal height tracks. The controller parameters of the next layer could be planned in advance by measuring the height of the current layer in real time to smooth out the unevenness. In Fig. 16, the microstructures of four typical segments are shown. These segments were observed during the controlled deposition process of the "bent pipe-shaped" part. The grain size underwent refinement from 5 to 15 μm to 3–10 μm , thereby demonstrating the effectiveness of the control strategy.

Miyagi et al. [97] captured the thermal radiation signal intensity of the melt pool, revealing its correlation with the width of the deposition layer and the laser power. As a result, an adaptive control system was developed. Figure 17 shows the control flow chart of the system. The laser power is adjusted to ensure a constant intensity of the thermal radiation signal, thereby avoiding excessive heat input. The target value of the thermal radiation signal can be flexibly changed during the deposition process, with an adaptive control cycle as high as 1 kHz. The effect of the control system is shown in Fig. 18, where it can be clearly seen that the deposition layer has a more accurate morphology and a more stable cross-section under the control of the system. Measurements also revealed a reduction in width variation from 63.6 to 12.5% compared to no adaptive shape control. Bi et al. [57, 123] constructed and tested a control system for DED-LB based on infrared temperature signals. The process-controlled samples had more uniform microstructure, hardness, and higher dimensional accuracy compared to multi-layer deposition using constant laser power. The PID controller designed by Farshidianfar et al. [124, 125] aims to maintain the cooling rate near the desired point by adjusting the scanning speed, thus ensuring a consistent controlled microstructure throughout the DED-LB process.

Beam shape is an equally important process parameter in addition to the laser power, scanning speed, and powder feed rate mentioned above. Beam shaping generally consists of adjusting the beam size and energy distribution. During

Fig. 16 The microstructures of Fe313 alloy in 4 typical segments [122]



DED-LB, the focusing of the laser beam changes the beam size and can regulate the heat input, which in turn affects the transient characteristics of the melt pool, the powder capture efficiency, and the microstructure of the sample [126, 127]. Zhao et al. [128] demonstrated the effect of the control of the focusing amount on the structure and properties of the samples by varying the amount of defocusing to achieve beam shaping. In addition, Wang et al. [129] used the layer height and defocus amount as the input and output parameters of the feedback control, respectively, to realize the real-time change of the beam size. The results showed that the designed control loop can effectively compensate for the height inconsistency problem during multi-layer deposition.

Other than controlling the beam size, beam shaping also involves adjusting the wavefront distribution of the laser to change the energy distribution and propagation characteristics. This type of shaping is realized by using a series of optical elements based on optical theory. Chen et al. [130] investigated the elemental polarization and the formation of Laves phases when depositing IN718 with a flat-topped laser beam (FTLB) versus a Gaussian distributed laser beam (GDLB). The results showed that the formation of Laves phase in GDLB-IN718 was significantly improved compared to FTLB-IN718. Shang et al. [131] used a variable beam profile modulator to change the energy distribution

to achieve the optimization of wear and thermal cracking resistance of the single-orbital deposition layer. However, the beam with heterogeneous energy distribution is difficult to be dynamically adjusted during processing due to the expensive optics and the difficulty of centralizing the optics in a laser head with a complex structure [132]. While limited research has been reported in this area due to hardware and software limitations, feedback control based on dynamic laser beam energy distribution adjustment is poised to become a future hotspot.

In addition to selecting appropriate control parameters, many reports also emphasize the importance of modeling the input and output mapping of the system. This modeling process serves as a basis for the design of the control system. Song et al. [34] developed a closed-loop control system, illustrated in Fig. 19, by establishing a state space model between laser power and melt pool temperature. By integrating this controller in series with the melt pool height controller and setting the corresponding control actions, Song et al. [35] developed a dual-input single-output controller. This setup effectively mitigated issues such as under-building and over-building in the multi-layer deposition process. The future temperature change could be predicted by such a generalized predictive controller (GPC) based on the real-time measured melt pool temperature. The establishment of

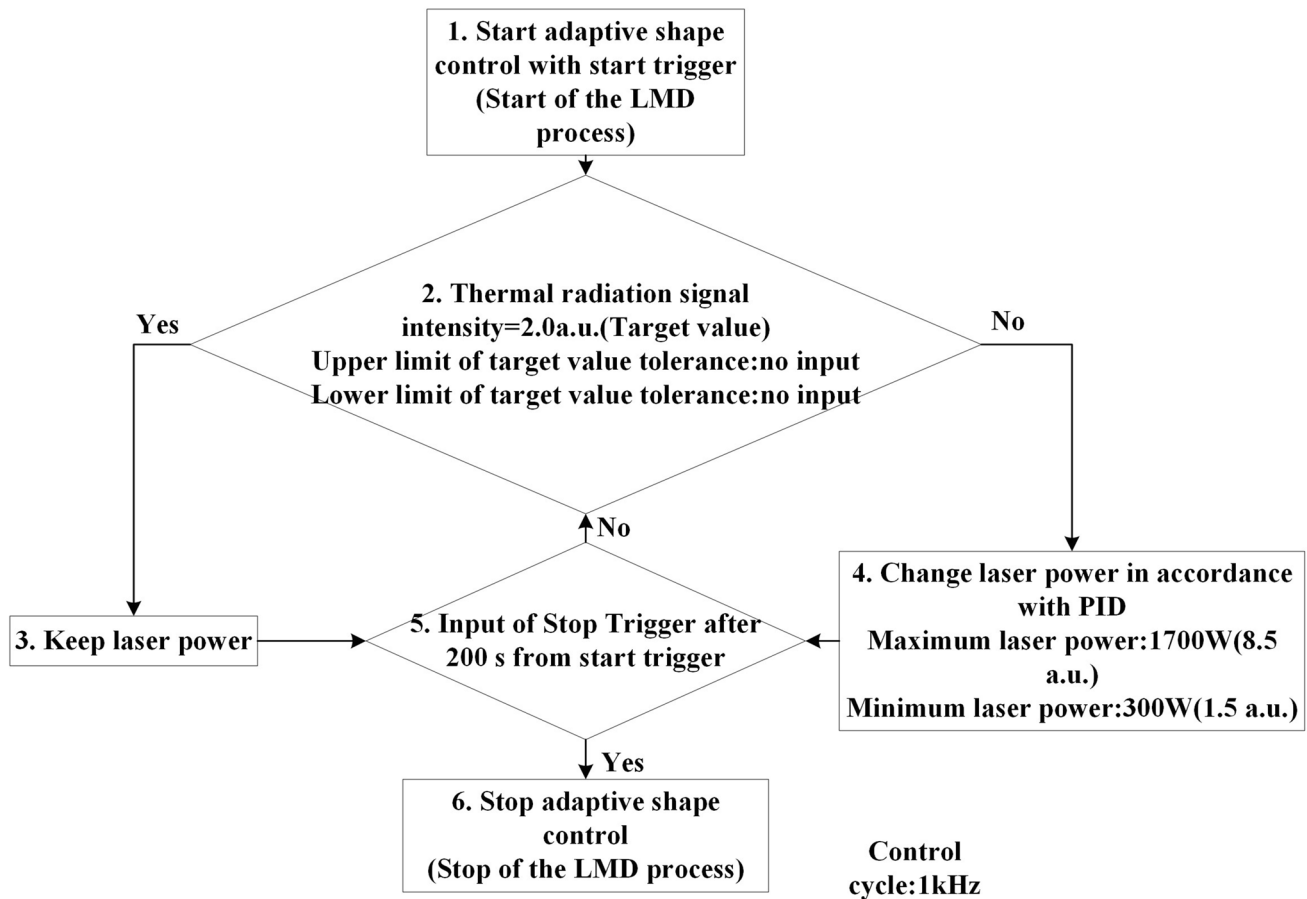


Fig. 17 Flow chart of adaptive shape control based on thermal radiation signal intensity [97]

the GPC temperature control system is of great significance for the future expansion of more complex multiple-input multiple-output (MIMO) DED-LB control systems. Based on a semi-empirical model named Hammerstein, Fathi et al. [133] established the dynamic response relationship between scanning speed and height. Subsequently, a joint control system consisting of a sliding mode controller (SMC) and a PID controller was developed on this basis. Experiments on the fabrication of ramp-shaped parts showed that the designed control system was able to effectively reduce the step effect. However, a maximum height deviation of 15% was still observed. Based on the method of isothermal migration, Devesse et al. [117] developed a dynamic thermophysical model of the melt pool and established the relationship between the surface temperature and width of the melt pool. This model subsequently informed the design of a DED-LB control system [134]. The control structure consisted of a static linear state feedback controller and a PI controller capable of adjusting the laser power to track changes in the width of the target melt pool within 40 ms with zero steady state error. As previously reported, conventional control methods are characterized by their simple structure and

effective control performance. However, large uncertainties persist when dealing with nonlinear, multivariate and time-varying DED-LB processes.

3.2 Intelligent optimization methods for control systems

Several researchers are integrating optimization algorithms and machine learning into DED-LB control systems to further improve control accuracy. We classify these intelligent optimization methods into two categories: optimization methods for constructing control models and optimization methods for tuning controller parameters. These methods play important roles before and during processing, respectively.

Machine learning algorithms such as neural networks, support vector regression (SVM), and optimization methods like genetic algorithms and PSO can be used to learn the nonlinear behavior of DED-LB systems from extensive amount of monitoring data. This enables the construction of more accurate, higher-order mapping models linking process parameters to the quality of the deposition. Ma et al. [135]

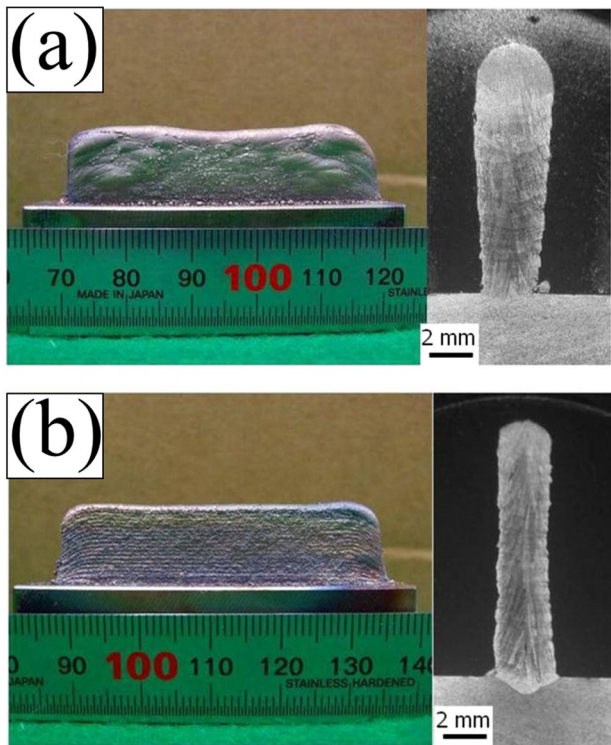


Fig. 18 Appearance and cross-sections of deposited wall structures (laser power = 1200 W, scanning velocity = 10 mm/s, $D_f = 36$ mm, $P_f = 0.01$ g/mm): (a) without adaptive shape control, (b) with adaptive shape control [97]

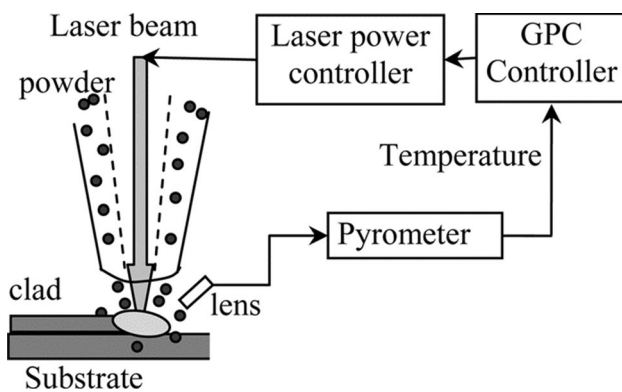


Fig. 19 Experimental setup of DMD process with a closed-loop temperature controller [34]

experimentally investigated the effect of different process parameters on dilution rate and residual stress. Subsequently, the optimal solution of the model response was obtained by applying multi-objective quantum particle swarm optimization (MOQPSO) under the constraints of a second-order polynomial response surface model. Yu et al. [136] developed a neural network model for genetic algorithm optimization between powder feeding rate, scanning speed,

and crack density. The experimental results showed that the genetic algorithm optimized the model prediction accuracy and obtained the best combination of process parameters at the minimum crack density. Similarly, Yang et al. [137] used a genetic algorithm to optimize the mapping model between laser power, scanning speed, and melt pool center temperature, based on which the optimal process parameters were obtained and validated for effectiveness. During the deposition process of 15-5PH powder with 20Cr13 substrate, Zhou et al. [138] established a prediction model for the geometrical characteristics of the deposition layer by combining the Grey Wolf Optimization (GWO) algorithm with BP neural network. The optimized best process parameters were laser power 1440 W, scanning speed 10 mm/s, and powder feeding rate 2.3 r/min. The deposition layer exhibited better microhardness and corrosion resistance compared to the pre-optimized deposition layer. There have been many reports of model prediction and process parameter optimization studies similar to these, which are oriented to different materials but have achieved good results [139–141].

According to the above, machine learning can be used to construct more accurate offline models. However, machine learning approaches that require multiple training and iterations can hardly meet the real-time demand of online control of DED-LB. Reports on machine learning models for online diagnosis and compensation of defects have just appeared recently. Gunasegaram et al. [142] pointed out the deficiencies of conventional closed-loop control strategies and proposed a machine learning framework for assisted processing in DED-LB. This framework addresses the gap in the direction of machine learning-assisted adaptive control. Pandiyan et al. [143] developed a self-supervised deep learning framework based on CNN and used a CCD camera to capture melt pool images, ultimately achieving effective classification of deposition quality. The possibility of real-time compensation in case of deviation during online monitoring was discussed by the developed predictive model. In conclusion, there are still limitations in terms of response speed and other aspects in integrating machine learning into online control strategies. Nevertheless, machine learning control methods with predictive capabilities can be more adaptable to the nonlinear and multivariate characteristics of DED-LB. It has great potential for future development.

Miao et al. [144] employed the optimization algorithm for tuning controller parameter. Specifically, the PSO algorithm was used to globally optimize the control power matrix of the linear quadratic regulator (LQR) to obtain the optimal control power matrix. The control strategy of PSO-LQR achieved a melt pool width control accuracy of 0.2 mm and a response time of 0.5 s in thin-wall processing. In order to avoid the cumbersome system identification process of conventional closed-loop control, Chen et al. [145] proposed a data-driven adaptive control strategy with automatic

parameter tuning capability based on the virtual reference feedback tuning (VRFT) algorithm. The parameters of the designed controller were updated in real time throughout the deposition process, regardless of the current time, layer, material, size, or shape. As can be seen from the experimental results shown in Fig. 20, the controller achieved a more uniform surface profile than conventional PID. Future research could explore expanding the control variables, such as powder feeding rate and scanning speed, to realize a more complete control system. Farshidianfar et al. [146] used the Adaptive Neuro-Fuzzy Inference System (ANFIS) algorithm to develop a mapping model of scanning speed to layer height. Based on the input-output data collected from

multiple sets of experiments, the model was identified and a control system for the DED-LB process was designed. The control system achieved satisfactory results in terms of response speed and stability compared to conventional controllers such as PID and MPC. Chen et al. [147] used a model-free self-organizing fuzzy control (SOFC) method for quality control, which is well adapted to the nonlinear coupling and time-varying characteristics of DED-LB. The SOFC controller had the ability to learn on-line and was able to adjust the laser power and scanning speed simultaneously. When faced with workpieces with geometrical and absorptive rate variations, the controller exhibited better immunity to interference than PID and fuzzy controllers.

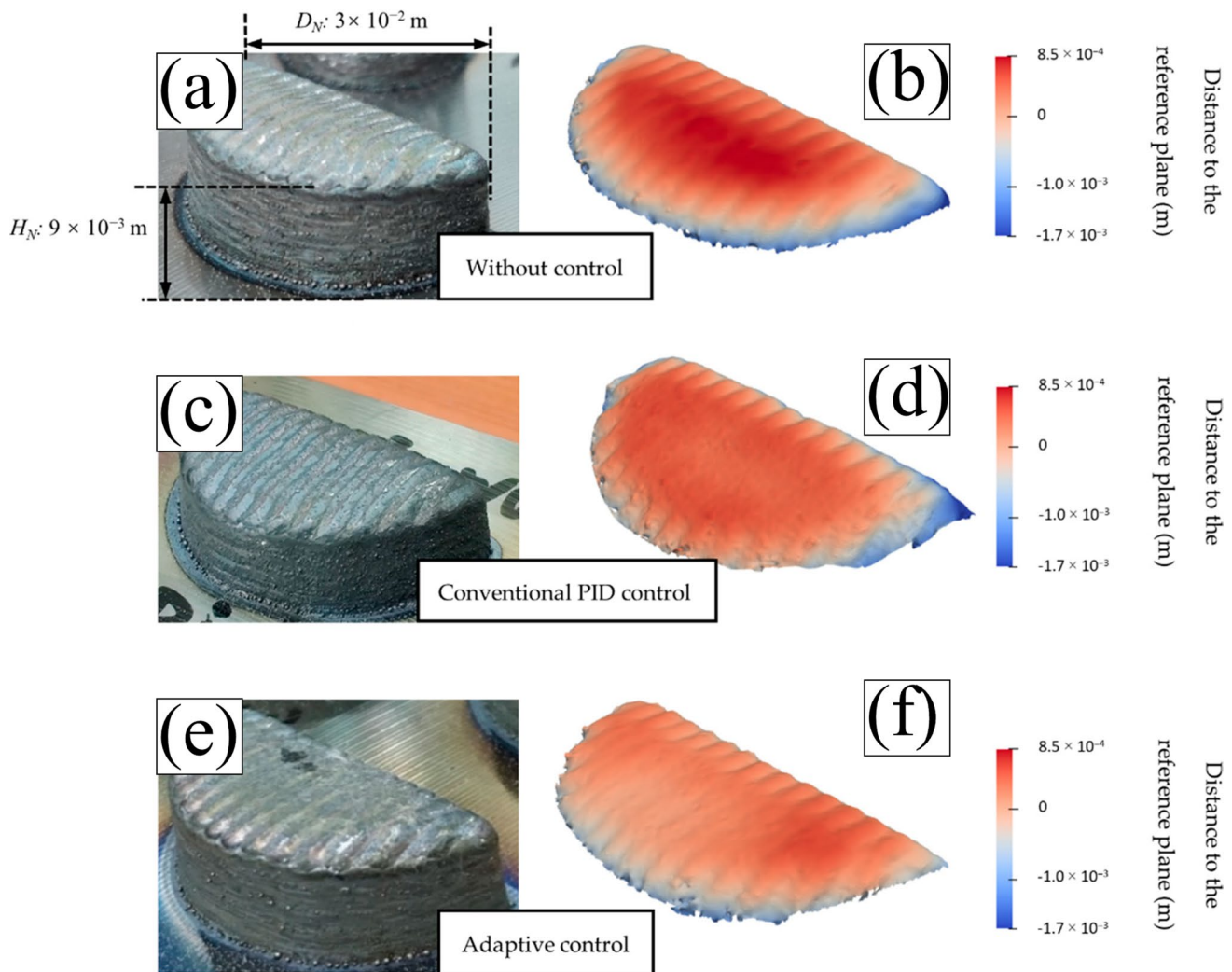


Fig. 20 Samples of experiment 1 (solid semicylinder with the profile tool path, 316 L stainless steel). **a** The sample fabricated without control. **b** The reconstructed surface of the uncontrolled sample. **c** The sample fabricated with a conventional proportional-integral-derivative (PID) controller. **d** The reconstructed surface of the conventional PID controlled sample. **e** The sample fabricated with the proposed adaptive controller. **f** The reconstructed surface of the adaptively controlled sample [145]

4 Existing main problems and future development trends

4.1 The main problems and limitations

DED-LB on-line monitoring techniques have been used to capture and quantify the time-varying characteristics of the process and establish mapping relationships between process parameters, monitoring signals and deposition quality. In addition, it can effectively reduce morphological and organizational defects through real-time feedback control. However, it is undeniable that there are still some problems to be solved.

4.1.1 Problems and limitations of on-line monitoring

As far as current on-line monitoring systems are concerned, they are either built on directly measurable features such as melt pool, powder, and substrate [74, 84], or indirectly characterized by spectral and acoustic signals to characterize small-scale evolutions of elemental compositions and defects during processing [96, 108]. However, these systems rarely operate at multiple scales. More advanced integrated sensing devices need further research and development.

Some on-line monitoring techniques may suffer from insufficient sensitivity and resolution in feature extraction and analysis. This is especially true when dealing with complex engineering problems such as DED-LB where strong radiation interference is coupled with multiple parameters, resulting in the inability to accurately capture and quantify microscopic changes.

X-ray imaging is an emerging on-line monitoring technique for DED-LB. Due to its strong penetration, it is able to reveal more in-depth information about the structural changes and defects generated during the process [48], but it also brings radiation safety issues and higher costs.

4.1.2 Problems and limitations of control strategies

Most of the control systems at this stage are limited to linear machining processes on flat surfaces. Due to the lack of control accuracy and stability, it cannot be applied to the machining of complex curved parts or coatings in actual production. Therefore, how to design a control system with higher accuracy and stability is a problem that needs to be solved.

On the other hand, most of the current closed-loop control studies regulate a single monitoring feature with a single process parameter, which cannot elucidate its complex forming mechanism and the dynamic evolutionary behavior of the melt pool under multi-field coupling. Even though Song

et al. [35] designed a multi-input system for layer height and temperature, it still fundamentally consists of the series connection of two single-input controllers.

4.2 Future research

The DED-LB process has multi-scale information such as surface morphology (macro-scale), cracks (meso-scale), and grain size (micro-scale). A single monitoring signal cannot guarantee the accuracy and comprehensiveness of the information. In order to adapt to the multi-field and multi-parameter coupling of DED-LB, the future on-line monitoring technology research should continuously improve on the existing monitoring equipment and develop integrated sensors with multi-information monitoring effects. By combining multiple monitoring means, a multimodal monitoring system can be created to provide more detailed information and feedback for the processing.

Both software and hardware are essential in enhancing the performance and functionality of on-line monitoring systems. Therefore, there is a need to explore multi-scale quality online assessment methods. For instance, a method that uses only a single sensor but realizes multi-scale mass monitoring to address macroscopic high instability and microscopic porosity was recently proposed by Li et al. [148]. A CMOS camera with optical feature enhancement techniques was employed to capture deposition profiles and melt pool images. Additionally, physical model-driven monitoring algorithms were designed to predict porosity. This provides a good research direction to revolutionize the multi-scale on-line monitoring technique.

Intelligent optimization methods have begun to be applied to pre-processing and processing of DED-LB. On the one hand, while these methods can enhance model accuracy through computer-experiment interaction [20], they may also introduce challenges such as insufficient response speed and lack of robustness [40]. Even though there are limited reports on their utilization for control system output input modeling, they indicate the future development of on-line control systems for DED-LB.

On the other hand, using the optimal solution obtained from the predictive model as an input for the initial process parameter combinations of the controller will result in a control system with faster convergence, higher control accuracy, and reduced cost. Furthermore, the optimized model can be used to develop a cloud database for storing information such as equipment status, historical data, and control commands [149, 150]. The control system developed based on the cloud database has powerful data storage and processing capabilities, which have already been applied in other engineering fields. This will provide valuable ideas for the improvement of DED-LB control systems.

Taken together, it is necessary to build a multi-sensor fusion on-line monitoring and control integrated DED-LB system in the future. As shown in Fig. 21, the image, temperature, plasma spectrum, acoustic emission, and X-ray signals collected by the on-line monitoring equipment are made to do real-time signal processing, from which the effective characteristic parameters are extracted and sent to the adaptive control system synchronously. In addition, intelligent optimization algorithms and advanced control strategies can be integrated into the control system model pre-processing and parameter tuning to reduce the response time while improving the control accuracy. Such a monitoring-control system has stronger information characterization capabilities and reduces post-processing costs. This will lay the foundation for deepening and expanding the application field of DED-LB.

5 Conclusion

This paper primarily focuses on the current development status of DED-LB, examining both on-line monitoring and process control. Through the above discussion and analysis of different monitoring signals, sensing devices, control

strategies and optimization algorithms, the following conclusions can be drawn:

1. Through the image, temperature, spectra, AE, and X-ray signals and a variety of monitoring equipment mentioned in this paper for on-line monitoring and signal processing, the process changes generated by DED-LB can be grasped in real time. It also provides more basis for quality regulation. In addition, through the process of closed-loop control, it can be found and recognized when the relevant defects immediately respond to avoid the quality problems caused by inappropriate process parameters. Therefore, on-line monitoring and real-time control play a pivotal role in optimizing and stabilizing DED-LB quality, enhancing production efficiency, and ensuring repeatability.
2. Most of the current on-line monitoring efforts are still limited to the use of a single monitoring device to obtain a single signal type, which cannot ensure the comprehensiveness and accuracy of the information. Future work should prioritize the integration of multi-sensor systems to achieve complementarity in terms of ability to acquire special information, sensitivity, accuracy, and anti-interference capability.

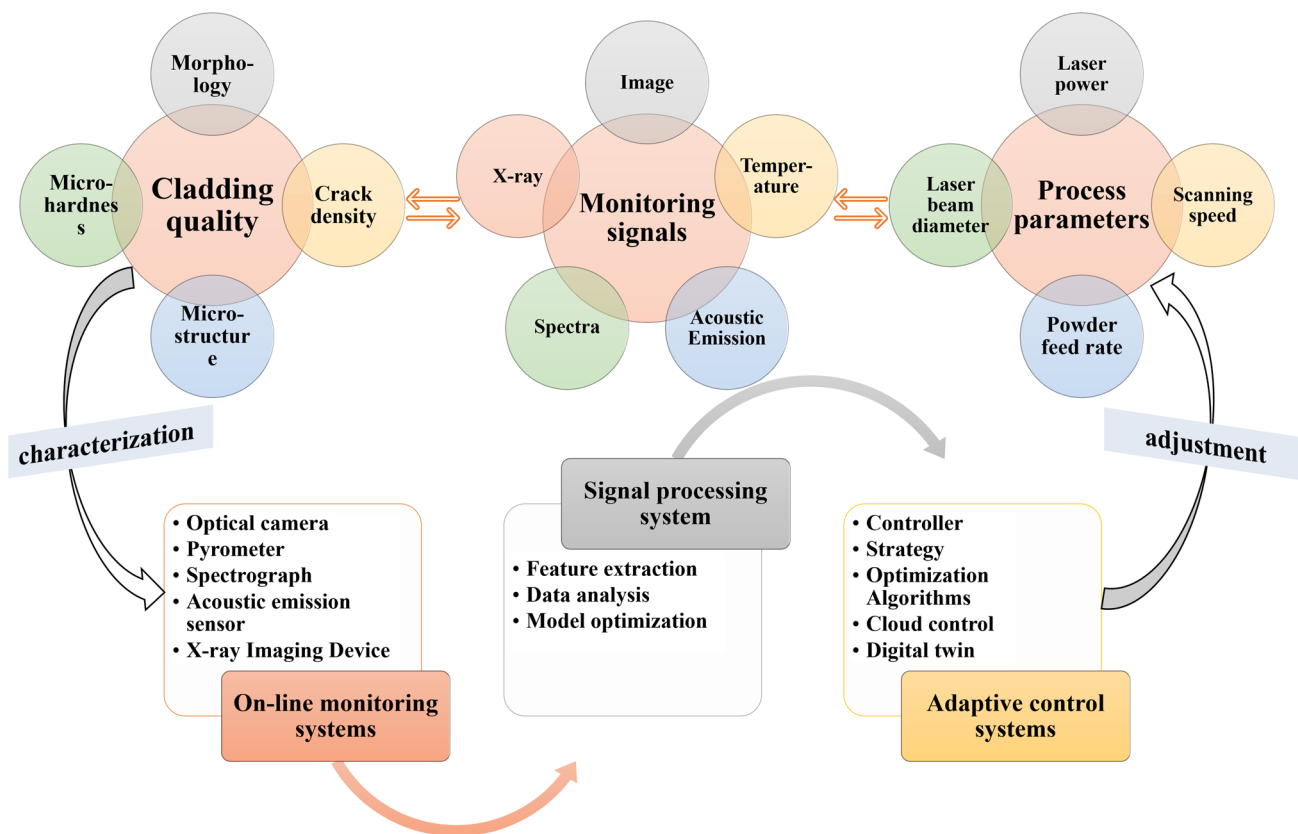


Fig. 21 Multi-sensor fusion for on-line monitoring of laser-directed energy deposition -adaptive system and parameter mapping relationship

3. Emerging technologies such as X-ray imaging, diffraction, and SAXS with stronger process information characterization capabilities have been gradually applied to DED-LB on-line monitoring. However, their utilization is limited by factors such as cost and specific operational requirements, necessitating the design of specialized DED-LB systems to accommodate them. Therefore, it is necessary to optimize the robustness of the monitoring equipment and the ability to extract and analyze data while working on the development of advanced on-line monitoring means.
4. Incorporating machine learning and optimization algorithms into the control strategy can significantly improve the control effect and quality stability. Even though few studies reported in this area, related works such as multi-parameter higher-order model prediction and offline process parameter optimization provide ideas for the improvement of DED-LB control strategies. Not only can the optimization algorithm be used for the tuning of controller parameters in adaptive control, but also the optimal solution obtained from the model incorporating the optimization algorithm can be used for the initial process parameter inputs to the controller. This leads to faster convergence speed and higher accuracy of the control system.
5. Control systems developed based on cloud database or digital twin are not old ways of quality regulation and prediction. Based on digital twin, Chen et al. [151] developed a multi-sensor fusion local quality prediction system using a coaxial camera, a microphone, and an off-axis short-wavelength infrared camera. In short, real-time monitoring and remote control can be realized through cloud database and digital twin, which are artificial intelligence products. At the same time, data sharing and collaboration between multiple users can be realized to promote the integrated, automated and intelligent development of DED-LB on-line monitoring and control technology.

Funding This research work was supported by the National Key Research and Development Program of China (Grant No. 2023YFB4606002), National Natural Science Foundation of China (Grant No. 52175455), University-Industry Collaborative Education Program of China (Grant No. 230800676014006), Liaoning Provincial Natural Science Foundation of China (Grant No. 2023-MSBA-006), and the Guangdong Provincial University Innovation Team Project (Grant No. 2020KCXTD012).

Data availability Transparent.

Code availability Not applicable.

Declarations

Competing interests The authors declare no competing interests.

References

1. Herzog D, Seyda V, Wycisk E, Emmelmann C (2016) Additive manufacturing of metals. *Acta Mater* 117:371–392. <https://doi.org/10.1016/j.actamat.2016.07.019>
2. Gong G, Ye J, Chi Y, Zhao Z, Wang Z, Xia G, Du X, Tian H, Yu H, Chen C (2021) Research status of laser additive manufacturing for metal: a review. *J Mater Res Technol* 15:855–884. <https://doi.org/10.1016/j.jmrt.2021.08.050>
3. Gusarov AV, Grigoriev SN, Volosova MA, Melnik YA, Laskin A, Kotoban DV, Okunkova AA (2018) On productivity of laser additive manufacturing. *J Mater Process Tech* 261:213–232. <https://doi.org/10.1016/j.jmatprotec.2018.05.033>
4. John M, Kuruveri UB, Menezes PL (2022) Laser cladding-based surface modification of carbon steel and high-alloy steel for extreme condition applications. *Coatings* 12:1444. <https://doi.org/10.3390/coatings12101444>
5. Lin P, Shen F, Wu K, Hwang S, Lee H (2020) Process optimization for directed energy deposition of SS316L components. *Int J Adv Manuf Technol* 111:1387–1400. <https://doi.org/10.1007/s00170-020-06113-z>
6. Vilar R (1999) Laser cladding. *J Laser Appl* 11:64–79. <https://doi.org/10.2351/1.521888>
7. Weng F, Chen C, Yu H (2014) Research status of laser cladding on titanium and its alloys: a review. *Mater Des* 58:412–425. <https://doi.org/10.1016/j.matdes.2014.01.077>
8. Shi B, Li T, Wang D, Zhang X, Zhang H (2021) Investigation on crack behavior of Ni60A alloy coating produced by coaxial laser cladding. *J Mater Sci* 56:13323–13336. <https://doi.org/10.1007/s10853-021-06108-5>
9. Fang L, Yao J, Hu X, Chai G (2011) Effect of laser power on the cladding temperature field and the heat affected zone. *J Iron Steel Res Int* 18:73–78. [https://doi.org/10.1016/S1006-706X\(11\)60014-9](https://doi.org/10.1016/S1006-706X(11)60014-9)
10. Liu Y, Zhang X, Zhang H, Li C, Cho HH, Li C (2023) Investigation on microstructure evolution of iron-based alloy via synchronous powder-feeding underwater laser additive. *Mater Des* 230:111985. <https://doi.org/10.1016/j.matdes.2023.111985>
11. Qi C, Zhan X, Gao Q, Liu L, Song Y, Li Y (2019) The influence of the pre-placed powder layers on the morphology, microscopic characteristics and microhardness of Ti-6Al-4V/WC MMC coatings during laser cladding. *Opt Laser Technol* 119:105572. <https://doi.org/10.1016/j.optlastec.2019.105572>
12. Bi G, Schürmann B, Gasser A, Wissenbach K, Poprawe R (2007) Development and qualification of a novel laser-cladding head with integrated sensors. *Int J Mach Tools Manuf* 47:555–561. <https://doi.org/10.1016/j.ijmactools.2006.05.010>
13. Li C, Yu Z, Gao J, Zhao J, Han X (2019) Numerical simulation and experimental study of cladding Fe60 on an ASTM 1045 substrate by laser cladding. *Surf Coat Technol* 357:965–977. <https://doi.org/10.1016/j.surfcoat.2018.10.099>
14. Zhu L, Xue P, Lan Q, Meng G, Ren Y, Yang Z, Xu P, Liu Z (2021) Recent research and development status of laser cladding: a review. *Opt Laser Technol* 138:106915. <https://doi.org/10.1016/j.optlastec.2021.106915>
15. Que L, Lian G, Yao M, Lu H (2022) Microstructure and properties of AlCoCrFeNiTi high-entropy alloy coatings prepared by laser cladding based on the response surface methodology. *Int*

- J Adv Manuf Technol 123:1307–1321. <https://doi.org/10.1007/s00170-022-10225-z>
16. Sexton L, Lavin S, Byrne G, Kennedy A (2002) Laser cladding of aerospace materials. *J Mater Process Tech* 122:63–68. [https://doi.org/10.1016/S0924-0136\(01\)01121-9](https://doi.org/10.1016/S0924-0136(01)01121-9)
 17. Bartkowski D, Młynarczyk A, Piasecki A, Dudziak B, Gościński M, Bartkowska A (2015) Microstructure, microhardness and corrosion resistance of Stellite-6 coatings reinforced with WC particles using laser cladding. *Opt Laser Technol* 68:191–201. <https://doi.org/10.1016/j.optlastec.2014.12.005>
 18. Liao T, Wang Z, Wu X, Liu Q, Guo Y, Ding K, Shang X (2023) Effect of V on microstructure, wear and corrosion properties in AlCoCrMoVx high entropy alloy coatings by laser cladding. *J Mater Res Technol* 23:4420–4431. <https://doi.org/10.1016/j.jmrt.2023.02.098>
 19. Kwok CT, Man HC, Cheng FT, Lo KH (2016) Developments in laser-based surface engineering processes: with particular reference to protection against cavitation erosion. *Surf Coat Technol* 291:189–204. <https://doi.org/10.1016/j.surfcoat.2016.02.019>
 20. Siddiqui AA, Dubey AK (2021) Recent trends in laser cladding and surface alloying. *Opt Laser Technol* 134:106619. <https://doi.org/10.1016/j.optlastec.2020.106619>
 21. Sundaraselvan S, Senthilkumar N, Tamizharasan T, Sait AN (2020) Surface modification of AZ61 magnesium alloy with nano TiO₂/Al₂O₃ using laser cladding technique. *Mater Today: Proc* 21:717–721. <https://doi.org/10.1016/j.matpr.2019.06.745>
 22. Deng Z, Liu D, Xiong Y, Zhu X, Li S, Liu J, Chen T (2022) Preparation of a hydroxyapatite–silver gradient bioactive ceramic coating with porous structure by laser cladding: a study of in vitro bioactivity. *Ceram Int* 48:30468–30481. <https://doi.org/10.1016/j.ceramint.2022.06.327>
 23. Zhang Y, Hu Y, Fang W, Li C, Wen Y (2023) Investigation of temperature field for the in-situ fabrication of particle-reinforced alumina ceramics coating via laser induction. *Appl Therm Eng* 228:120446. <https://doi.org/10.1016/j.applthermaleng.2023.120446>
 24. Wang K, Liu W, Hong Y, Sohan HS, Tong Y, Hu Y, Zhang M, Zhang J, Xiang D, Fu H (2023) An overview of technological parameter optimization in the case of laser cladding. *Coatings* 13:496. <https://doi.org/10.3390/coatings13030496>
 25. Herzog T, Brandt M, Trinchi A, Sola A, Molotnikov A (2023) Process monitoring and machine learning for defect detection in laser-based metal additive manufacturing. *J Intell Manuf* 1–31. <https://doi.org/10.1007/s10845-023-02119-y>
 26. Li W, Liu W, Saleheen KM, Liu H, Xia Y, Al-Hammadi G, Xue L, Wang F, Song X, Zhang Y (2023) Research and prospect of on-line monitoring technology for laser additive manufacturing. *Int J Adv Manuf Technol* 125:25–46. <https://doi.org/10.1007/s00170-022-10758-3>
 27. Kahlen F, Kar A (2001) Tensile strengths for laser-fabricated parts and similarity parameters for rapid manufacturing. *J Manuf Sci Eng* 123:38–44. <https://doi.org/10.1115/1.1286472>
 28. Shepeleva L, Medres B, Kaplan WD, Bamberger M, Weisheit A (2000) Laser cladding of turbine blades. *Surf Coat Technol* 125:45–48. [https://doi.org/10.1016/S0257-8972\(99\)00603-9](https://doi.org/10.1016/S0257-8972(99)00603-9)
 29. Qiu X, Liu C (2013) Microstructure and properties of Al₂Cr-FeCoCuTiNi high-entropy alloys prepared by laser cladding. *J Alloy Compd* 553:216–220. <https://doi.org/10.1016/j.jallcom.2012.11.100>
 30. Yan X, Dong S, Xu B, Cao Y (2018) Progress and challenges of ultrasonic testing for stress in remanufacturing laser cladding coating. *Materials* 11:293. <https://doi.org/10.3390/ma11020293>
 31. Song J, Deng Q, Chen C, Hu D, Li Y (2006) Rebuilding of metal components with laser cladding forming. *Appl Surf Sci* 252:7934–7940. <https://doi.org/10.1016/j.apsusc.2005.10.025>
 32. Thawari N, Gullipalli C, Katiyar JK, Gupta T (2023) In-process monitoring of distortion and temperature in multi-layer laser cladding of Stellite 6 and Inconel 718 alloys. *Proc Inst Mech Eng Pt B J Eng* 237:3–15. <https://doi.org/10.1177/09544054221092937>
 33. Muvvala G, Mullick S, Nath AK (2020) Development of process maps based on molten pool thermal history during laser cladding of Inconel 718/TiC metal matrix composite coatings. *Surf Coat Technol* 399:126100. <https://doi.org/10.1016/j.surfcoat.2020.126100>
 34. Song L, Mazumder J (2010) Feedback control of melt pool temperature during laser cladding process. *Ieee T Contr Syst Technol* 19:1349–1356. <https://doi.org/10.1109/TCST.2010.2093901>
 35. Song L, Bagavath-Singh V, Dutta B, Mazumder J (2012) Control of melt pool temperature and deposition height during direct metal deposition process. *Int J Adv Manuf Technol* 58:247–256. <https://doi.org/10.1007/s00170-011-3395-2>
 36. Xu H, Huang H (2023) In situ monitoring in laser melt injection based on fusion of infrared thermal and high-speed camera images. *J Manuf Process* 92:466–478. <https://doi.org/10.1016/j.jmapro.2023.02.059>
 37. Colodrón P, Fariña J, Rodríguez-Andina JJ, Vidal F, Mato JL, Montealegre MÁ (2011) Performance improvement of a laser cladding system through FPGA-based control, IECON 2011-37th Annual Conference of the IEEE Industrial Electronics Society, IEEEC, 2814–2819. <https://doi.org/10.1109/IECON.2011.6119758>
 38. Hsu H, Lo Y, Lee M (2019) Vision-based inspection system for cladding height measurement in Direct Energy Deposition (DED). *Addit Manuf* 27:372–378. <https://doi.org/10.1016/j.addma.2019.03.017>
 39. Smurov I, Doubenskaia M, Grigoriev S, Nazarov A (2012) Optical monitoring in laser cladding of Ti6Al4V. *J Therm Spray Technol* 21:1357–1362. <https://doi.org/10.1007/s11666-012-9808-4>
 40. Hofman JT, Pathiraj B, Van Dijk J, De Lange DF, Meijer J (2012) A camera based feedback control strategy for the laser cladding process. *J Mater Process Tech* 212:2455–2462. <https://doi.org/10.1016/j.jmatprotec.2012.06.027>
 41. Muvvala G, Karmakar DP, Nath AK (2017) Online assessment of TiC decomposition in laser cladding of metal matrix composite coating. *Mater Des* 121:310–320. <https://doi.org/10.1016/j.matdes.2017.02.061>
 42. Sampson R, Lancaster R, Sutcliffe M, Carswell D, Hauser C, Barras J (2020) An improved methodology of melt pool monitoring of direct energy deposition processes. *Opt Laser Technol* 127:106194. <https://doi.org/10.1016/j.optlastec.2020.106194>
 43. Muvvala G, Karmakar DP, Nath AK (2018) In-process detection of microstructural changes in laser cladding of in-situ inconel 718/TiC metal matrix composite coating. *J Alloy Compd* 740:545–558. <https://doi.org/10.1016/j.jallcom.2017.12.364>
 44. Chen Y, Clark SJ, Sinclair L, Leung CLA, Marussi S, Connolley T, Atwood RC, Baxter GJ, Jones MA, Todd I (2021) Synchrotron X-ray imaging of directed energy deposition additive manufacturing of titanium alloy. Ti-6242. *Addit Manuf*. 41:101969. <https://doi.org/10.1016/j.addma.2021.101969>
 45. Chen Y, Clark SJ, Collins DM, Marussi S, Hunt SA, Fenech DM, Connolley T, Atwood RC, Magdysyuk OV, Baxter GJ (2021) Correlative synchrotron X-ray imaging and diffraction of directed energy deposition additive manufacturing. *Acta Mater* 209:116777. <https://doi.org/10.1016/j.actamat.2021.116777>
 46. Ren W, Mazumder J (2020) In-situ porosity recognition for laser additive manufacturing of 7075-Al alloy using plasma emission spectroscopy. *Sci Rep* 10:19493. <https://doi.org/10.1038/s41598-020-75131-4>

47. Song L, Wang F, Li S, Han X (2017) Phase congruency melt pool edge extraction for laser additive manufacturing. *J Mater Process Tech* 250:261–269. <https://doi.org/10.1016/j.jmatprotec.2017.07.013>
48. Wolff SJ, Webster S, Parab ND, Aronson B, Gould B, Greco A, Sun T (2021) In-situ observations of directed energy deposition additive manufacturing using high-speed X-ray imaging. *JOM-US* 73:189–200. <https://doi.org/10.1007/s11837-020-04469-x>
49. Lindenmeyer A, Webster S, Zaeh MF, Ehmann KF, Cao J (2021) Template-bayesian approach for the evaluation of melt pool shape and dimension of a DED-process from in-situ X-ray images. *CIRP Ann* 70:183–186. <https://doi.org/10.1016/j.cirp.2021.03.011>
50. Gaja H, Liou F (2018) Defect classification of laser metal deposition using logistic regression and artificial neural networks for pattern recognition. *Int J Adv Manuf Technol* 94:315–326. <https://doi.org/10.1007/s00170-017-0878-9>
51. Gaja H, Liou F (2017) Defects monitoring of laser metal deposition using acoustic emission sensor. *Int J Adv Manuf Technol* 90:561–574. <https://doi.org/10.1007/s00170-016-9366-x>
52. Yan Z, Liu W, Tang Z, Liu X, Zhang N, Wang Z, Zhang H (2019) Effect of thermal characteristics on distortion in laser cladding of AISI 316L. *J Manuf Process* 44:309–318. <https://doi.org/10.1016/j.jmapro.2019.06.011>
53. Khanzadeh M, Tian W, Yadollahi A, Doude HR, Tschopp MA, Bian L (2018) Dual process monitoring of metal-based additive manufacturing using tensor decomposition of thermal image streams. *Addit Manuf* 23:443–456. <https://doi.org/10.1016/j.addma.2018.08.014>
54. Liu S, Farahmand P, Kovacevic R (2014) Optical monitoring of high power direct diode laser cladding. *Opt Laser Technol* 64:363–376. <https://doi.org/10.1016/j.optlastec.2014.06.002>
55. Ocelik V, Bosgra J, de Hosson JTM (2009) In-situ strain observation in high power laser cladding. *Surf Coat Technol* 203:3189–3196. <https://doi.org/10.1016/j.surfcoat.2009.03.050>
56. Smurov I, Doubenskaia M Temperature monitoring by optical methods in laser processing, *Laser-Assisted Fabrication of Materials*, Springer 2012. 375–422. https://doi.org/10.1007/978-3-642-28359-8_9
57. Bi G, Gasser A, Wissenbach K, Drenker A, Poprawe R (2006) Identification and qualification of temperature signal for monitoring and control in laser cladding. *Opt Laser Eng* 44:1348–1359. <https://doi.org/10.1016/j.optlaseng.2006.01.009>
58. Lin J, Steen WM (1998) Design characteristics and development of a nozzle for coaxial laser cladding. *J Laser Appl* 10:55–63. <https://doi.org/10.2351/1.521821>
59. Aragon C, Madurga V, Aguilera JA (2002) Application of laser-induced breakdown spectroscopy to the analysis of the composition of thin films produced by pulsed laser deposition. *Appl Surf Sci* 197:217–223. [https://doi.org/10.1016/S0169-4332\(02\)00368-9](https://doi.org/10.1016/S0169-4332(02)00368-9)
60. Fortes FJ, Moros J, Lucena P, Cabalín LM, Laserna JJ (2013) Laser-induced breakdown spectroscopy. *ANAL CHEM* 85:640–669. <https://doi.org/10.1021/ac303220r>
61. De Baere D, Devesse W, De Pauw B, Smeesters L, Thienpont H, Guillaume P (2016) Spectroscopic monitoring and melt pool temperature estimation during the laser metal deposition process. *J Laser Appl* 28. <https://doi.org/10.2351/1.4943995>
62. Yue HH, Qin SJ, Markle RJ, Nauert C, Gatto M (2000) Fault detection of plasma etchers using optical emission spectra. *IEEE Trans Semicond Manuf* 13:374–385. <https://doi.org/10.1109/66.857948>
63. Scruby CB (1987) An introduction to acoustic emission. *J Phys E* 20:946. <https://doi.org/10.1088/0022-3735/20/8/001>
64. Lhuissier P, Bataillon X, Maestre C, Sijobert J, Cabrol E, Bertrand P, Boller E, Rack A, Blandin J, Salvo L (2020) In situ 3D X-ray microtomography of laser-based powder-bed fusion (L-PBF)—A feasibility study. *ADDIT MANUF* 34:101271. <https://doi.org/10.1016/j.addma.2020.101271>
65. Wolff SJ, Wu H, Parab N, Zhao C, Ehmann KF, Sun T, Cao J (2019) In-situ high-speed X-ray imaging of piezo-driven directed energy deposition additive manufacturing. *Sci Rep* 9:962. <https://doi.org/10.1038/s41598-018-36678-5>
66. De La Garcia A, Pflieger M, Aramendi B, Cabeza M, Zubiri F, Mitter T, Reitingger B, Scherleitner E (2019) Online cracking detection by means of optical techniques in laser-cladding process. *Struct Control Health Monit* 26:e2291. <https://doi.org/10.1002/stc.2291>
67. Svetlizky D, Das M, Zheng B, Vyatskikh AL, Bose S, Bandyopadhyay A, Schoenung JM, Lavernia EJ, Eliaz N (2021) Directed energy deposition (DED) additive manufacturing: physical characteristics, defects, challenges and applications. *Mater Today* 49:271–295. <https://doi.org/10.1016/j.mattod.2021.03.020>
68. Ren Z, Gao L, Clark SJ, Fezzaa K, Shevchenko P, Choi A, Everhart W, Rollett AD, Chen L, Sun T (2023) Machine learning-aided real-time detection of keyhole pore generation in laser powder bed fusion. *Science* 379:89–94. <https://doi.org/10.1126/science.add4667>
69. Zhao C, Fezzaa K, Cunningham RW, Wen H, De Carlo F, Chen L, Rollett AD, Sun T (2017) Real-time monitoring of laser powder bed fusion process using high-speed X-ray imaging and diffraction. *Sci Rep* 7:3602. <https://doi.org/10.1038/s41598-017-03761-2>
70. Liu W, Tang Z, Liu X, Wang H, Zhang H (2017) A review on in-situ monitoring and adaptive control technology for laser cladding remanufacturing. *Procedia Cirp* 61:235–240. <https://doi.org/10.1016/j.procir.2016.11.217>
71. Sun Z, Guo W, Li L (2020) In-process measurement of melt pool cross-sectional geometry and grain orientation in a laser directed energy deposition additive manufacturing process. *Opt Laser Technol* 129:106280. <https://doi.org/10.1016/j.optlastec.2020.106280>
72. Moralejo S, Penaranda X, Nieto S, Barrios A, Arrizubieta I, Tabernerero I, Figueras J (2017) A feedforward controller for tuning laser cladding melt pool geometry in real time. *Int J Adv Manuf Technol* 89:821–831. <https://doi.org/10.1007/s00170-016-9138-7>
73. Hofman JT, De Lange DF, Pathiraj B, Meijer J (2011) FEM modeling and experimental verification for dilution control in laser cladding. *J Mater Process Tech* 211:187–196. <https://doi.org/10.1016/j.jmatprotec.2010.09.007>
74. Lei K, Qin X, Liu H, Ni M (2018) Analysis and modeling of melt pool morphology for high power diode laser cladding with a rectangle beam spot. *Opt Laser Eng* 110:89–99. <https://doi.org/10.1016/j.optlaseng.2018.05.022>
75. Donadello S, Motta M, Demir AG, Previtali B (2019) Monitoring of laser metal deposition height by means of coaxial laser triangulation. *Opt Laser Eng* 112:136–144. <https://doi.org/10.1016/j.optlaseng.2018.09.012>
76. Irvani-Tabrizipour M, Toyserkani E (2007) An image-based feature tracking algorithm for real-time measurement of clad height. *Mach Vis Appl* 18:343–354. <https://doi.org/10.1007/s00138-006-0066-7>
77. Yan J, Xu Z, Wu Z, Li Q, Tang M, Ling J (2021) Edge detection method of laser cladding pool image based on morphology, *AOPC 2021: Advanced Laser Technology and Applications*, SPIE, 246–253. <https://doi.org/10.1117/12.2606710>
78. Kao I, Hsu Y, Lai YH, Perng J (2019) Laser cladding quality monitoring using coaxial image based on machine learning. *IEEE Trans Instrum Meas* 69:2868–2880. <https://doi.org/10.1109/TIM.2019.2926878>
79. Zhang Y, Shen S, Li H, Hu Y (2022) Review of in situ and real-time monitoring of metal additive manufacturing based on image

- processing. *Int J Adv Manuf Technol* 123:1–20. <https://doi.org/10.1007/s00170-022-10178-3>
80. Farahmand P, Kovacevic R (2014) An experimental–numerical investigation of heat distribution and stress field in single-and multi-track laser cladding by a high-power direct diode laser. *Opt Laser Technol* 63:154–168. <https://doi.org/10.1016/j.optlastec.2014.04.016>
 81. Köhler H, Thomy C, Vollertsen F (2016) Contact-less temperature measurement and control with applications to laser cladding. *Weld World* 60:1–9. <https://doi.org/10.1007/s40194-015-0275-7>
 82. Leonidas E, Ayvar-Soberanis S, Laalej H, Fitzpatrick S, Willmott JR (2022) A comparative review of thermocouple and infrared radiation temperature measurement methods during the machining of metals. *Sensors-Basel* 22:4693. <https://doi.org/10.3390/s22134693>
 83. Thawari N, Gullipalli C, Gupta T (2023) Effect of buffer layer on distortion and temperature in laser cladding. *Mater Today: Proc* 72:1792–1797. <https://doi.org/10.1016/j.matpr.2022.09.573>
 84. Thawari N, Gullipalli C, Vanmore H, Gupta T (2022) In-situ monitoring and modelling of distortion in multi-layer laser cladding of stellite 6: parametric and numerical approach. *Mater Today Commun* 33:104751. <https://doi.org/10.1016/j.mtcomm.2022.104751>
 85. Srisungsthisunti P, Kaewprachum B, Yang Z, Gao G (2022) Real-time quality monitoring of laser cladding process on rail steel by an infrared camera. *Metals-Basel* 12:825. <https://doi.org/10.3390/met12050825>
 86. Muvvala G, Karmakar DP, Nath AK (2017) Online monitoring of thermo-cycles and its correlation with microstructure in laser cladding of nickel based super alloy. *Opt Laser Eng* 88:139–152. <https://doi.org/10.1016/j.optlaseng.2016.08.005>
 87. Doubenskaia M, Pavlov M, Grigoriev S, Smurov I (2013) Definition of brightness temperature and restoration of true temperature in laser cladding using infrared camera. *Surf Coat Technol* 220:244–247. <https://doi.org/10.1016/j.surfcoat.2012.10.044>
 88. Tang L, Landers RG (2010) Melt pool temperature control for laser metal deposition processes—part I: online temperature control. *J Manuf Sci Eng* 132. <https://doi.org/10.1115/1.4000882>
 89. Salehi D, Brandt M (2006) Melt pool temperature control using LabVIEW in nd: YAG laser blown powder cladding process. *Int J Adv Manuf Technol* 29:273–278. <https://doi.org/10.1007/s00170-005-2514-3>
 90. Tang L, Landers RG (2010) Melt pool temperature control for laser metal deposition processes—part II: layer-to-layer temperature control. *J Manuf Sci Eng* 132. <https://doi.org/10.1115/1.4000883>
 91. Tang Z, Liu W, Wang Y, Saleheen KM, Liu Z, Peng S, Zhang Z, Zhang H (2020) A review on in situ monitoring technology for directed energy deposition of metals. *Int J Adv Manuf Technol* 108:3437–3463. <https://doi.org/10.1007/s00170-020-05569-3>
 92. Song L, Huang W, Han X, Mazumder J (2016) Real-time composition monitoring using support vector regression of laser-induced plasma for laser additive manufacturing. *IEEE Trans Ind Electron* 64:633–642. <https://doi.org/10.1109/TIE.2016.2608318>
 93. Choi J, Wooldridge M, Mazumder J (2023) Spectroscopy-based smart optical monitoring system in the applications of laser additive manufacturing. *J Laser Appl* 35. <https://doi.org/10.2351/7.0000910>
 94. Ni C, Shi Y, Liu J, Huang G (2018) Characterization of Al₀.5FeCu₀.7NiCoCr high-entropy alloy coating on aluminum alloy by laser cladding. *Opt Laser Technol* 105:257–263. <https://doi.org/10.1016/j.optlastec.2018.01.058>
 95. Shin J, Mazumder J (2018) Composition monitoring using plasma diagnostics during direct metal deposition (DMD) process. *Opt Laser Technol* 106:40–46. <https://doi.org/10.1016/j.optlastec.2018.03.020>
 96. Lednev VN, Sdvizhenskii PA, Stavertiy AY, Grishin MY, Tretyakov RS, Asyutin RD, Pershin SM (2021) Online and in situ laser-induced breakdown spectroscopy for laser welding monitoring. *Spectrochimica Acta Part B: at Spectrosc* 175:106032. <https://doi.org/10.1016/j.sab.2020.106032>
 97. Miyagi M, Tsukamoto T, Kawanaka H (2014) Adaptive shape control of laser-deposited metal structures by adjusting Weld pool size. *J Laser Appl* 26. <https://doi.org/10.2351/1.4869499>
 98. Sdvizhenskii PA, Lednev VN, Asyutin RD, Grishin MY, Tretyakov RS, Pershin SM (2020) Online laser-induced breakdown spectroscopy for metal-particle powder flow analysis during additive manufacturing. *J Anal Atom Spectrom* 35:246–253. <https://doi.org/10.1039/C9JA00343F>
 99. Lednev VN, Sdvizhenskii PA, Asyutin RD, Tretyakov RS, Grishin MY, Stavertiy AY, Pershin SM (2019) In situ multi-elemental analysis by laser induced breakdown spectroscopy in additive manufacturing. *Addit Manuf* 25:64–70. <https://doi.org/10.1016/j.addma.2018.10.043>
 100. Song L, Mazumder J (2011) Real time cr measurement using optical emission spectroscopy during direct metal deposition process. *IEEE SENS J* 12:958–964. <https://doi.org/10.1109/JSEN.2011.2162316>
 101. Kong F, Kovacevic R (2010) Modeling of heat transfer and fluid flow in the laser multilayered cladding process. *Metall Mater Trans B* 41:1310–1320. <https://doi.org/10.1007/s11663-010-9412-2>
 102. Wang S, Liu C (2019) Real-time monitoring of chemical composition in nickel-based laser cladding layer by emission spectroscopy analysis. *Materials* 12:2637. <https://doi.org/10.3390/ma12162637>
 103. Lu QY, Wong CH (2018) Additive manufacturing process monitoring and control by non-destructive testing techniques: challenges and in-process monitoring. *Virtual Phys Prototyp* 13:39–48. <https://doi.org/10.1080/17452759.2017.1351201>
 104. Kordatos EZ, Aggelis DG, Matikas TE (2012) Monitoring mechanical damage in structural materials using complimentary NDE techniques based on thermography and acoustic emission. *Compos Part B: Eng* 43:2676–2686. <https://doi.org/10.1016/j.compositesb.2011.12.013>
 105. Li K, Li T, Ma M, Wang D, Deng W, Lu H (2021) Laser cladding state recognition and crack defect diagnosis by acoustic emission signal and neural network. *Opt Laser Technol* 142:107161. <https://doi.org/10.1016/j.optlastec.2021.107161>
 106. Taheri H, Koester LW, Bigelow TA, Faierson EJ, Bond LJ (2019) In situ additive manufacturing process monitoring with an acoustic technique: clustering performance evaluation using K-means algorithm. *J Manuf Sci Eng* 141:041011. <https://doi.org/10.1115/1.4042786>
 107. Whiting J, Springer A, Sciammarella F (2018) Real-time acoustic emission monitoring of powder mass flow rate for directed energy deposition. *ADDIT MANUF* 23:312–318. <https://doi.org/10.1016/j.addma.2018.08.015>
 108. Wang F, Mao H, Zhang D, Zhao X, Shen Y (2008) Online study of cracks during laser cladding process based on acoustic emission technique and finite element analysis. *Appl Surf Sci* 255:3267–3275. <https://doi.org/10.1016/j.apsusc.2008.09.039>
 109. Strantzla M, Van Hemelrijck D, Guillaume P, Aggelis DG (2017) Acoustic emission monitoring of crack propagation in additively manufactured and conventional titanium components. *MECH RES COMMUN* 84:8–13. <https://doi.org/10.1016/j.mechrescom.2017.05.009>
 110. Li Y, Xu F (2021) Structural condition monitoring and identification of laser cladding metallic panels based on an acoustic emission signal feature optimization algorithm. *Struct Health Monit* 20:1052–1073. <https://doi.org/10.1177/1475921720945637>

111. Wolff SJ, Wang H, Gould B, Parab N, Wu Z, Zhao C, Greco A, Sun T (2021) In situ X-ray imaging of pore formation mechanisms and dynamics in laser powder-blown directed energy deposition additive manufacturing. *Int J Mach Tools Manuf* 166:103743. <https://doi.org/10.1016/j.ijmactools.2021.103743>
112. Ioannidou C, König H, Semjatov N, Ackelid U, Staron P, Koerner C, Hedström P, Lindwall G (2022) In-situ synchrotron X-ray analysis of metal Additive Manufacturing: current state, opportunities and challenges. *MATER Des* 219:110790. <https://doi.org/10.1016/j.matdes.2022.110790>
113. Tapia G, Elwany A (2014) A review on process monitoring and control in metal-based additive manufacturing. *J Manuf Sci Eng* 136:060801. <https://doi.org/10.1115/1.4028540>
114. Reutzel EW, Nassar AR (2015) A survey of sensing and control systems for machine and process monitoring of directed-energy, metal-based additive manufacturing. *RAPID Prototyp J* 21:159–167. <https://doi.org/10.1108/RPJ-12-2014-0177>
115. Dumanidis C, Kwak Y (2001) Geometry modeling and control by infrared and laser sensing in thermal manufacturing with material deposition. *J Manuf Sci Eng* 123:45–52. <https://doi.org/10.1115/1.1344898>
116. Pinkerton AJ, Li L (2004) Modelling the geometry of a moving laser melt pool and deposition track via energy and mass balances. *J Phys D* 37:1885. <https://doi.org/10.1088/0022-3727/37/14/003>
117. Devesse W, De Baere D, Guillaume P (2014) The isotherm migration method in spherical coordinates with a moving heat source. *Int J Heat Mass Transf* 75:726–735. <https://doi.org/10.1016/j.ijheatmasstransfer.2014.04.015>
118. Yang Q, Yuan Z, Zhi X, Yan Z, Tian H, Chen X (2020) Real-time width control of molten pool in laser engineered net shaping based on dual-color image. *Opt Laser Technol* 123:105925. <https://doi.org/10.1016/j.optlastec.2019.105925>
119. Akbari M, Kovacevic R (2019) Closed loop control of melt pool width in robotized laser powder-directed energy deposition process. *Int J Adv Manuf Technol* 104:2887–2898. <https://doi.org/10.1007/s00170-019-04195-y>
120. Ding Y, Warton J, Kovacevic R (2016) Development of sensing and control system for robotized laser-based direct metal addition system. *ADDIT MANUF* 10:24–35. <https://doi.org/10.1016/j.addma.2016.01.002>
121. Fathi A, Khajepour A, Toyserkani E, Durali M (2007) Clad height control in laser solid freeform fabrication using a feed-forward PID controller. *Int J Adv Manuf Technol* 35:280–292. <https://doi.org/10.1007/s00170-006-0721-1>
122. Shi T, Shi J, Xia Z, Lu B, Shi S, Fu G (2020) Precise control of variable-height laser metal deposition using a height memory strategy. *J MANUF PROCESS* 57:222–232. <https://doi.org/10.1016/j.jmapro.2020.05.026>
123. Bi G, Gasser A, Wissenbach K, Drenker A, Poprawe R (2006) Characterization of the process control for the direct laser metallic powder deposition. *Surf Coat Technol* 201:2676–2683. <https://doi.org/10.1016/j.surfcoat.2006.05.006>
124. Farshidianfar MH, Khajepour A, Gerlich AP (2016) Effect of real-time cooling rate on microstructure in laser additive manufacturing. *J MATER PROCESS TECH* 231:468–478. <https://doi.org/10.1016/j.jmatprotec.2016.01.017>
125. Farshidianfar MH, Khajepour A, Gerlich A (2016) Real-time control of microstructure in laser additive manufacturing. *Int J Adv Manuf Technol* 82:1173–1186. <https://doi.org/10.1007/s00170-015-7423-5>
126. Xiong Y, Smugersky JE, Schoenung JM (2009) The influence of working distance on laser deposited WC-Co. *J MATER PROCESS TECH* 209:4935–4941. <https://doi.org/10.1016/j.jmatprotec.2009.01.016>
127. Haley JC, Zheng B, Bertoli US, Dupuy AD, Schoenung JM, Lavernia EJ (2019) Working distance passive stability in laser directed energy deposition additive manufacturing. *MATER Des* 161:86–94. <https://doi.org/10.1016/j.matdes.2018.11.021>
128. Zhao Y, Sun W, Wang Q, Sun Y, Chen J, Du C, Xing H, Li N, Tian W (2023) Effect of beam energy density characteristics on microstructure and mechanical properties of Nickel-based alloys manufactured by laser directed energy deposition. *J MATER PROCESS TECH* 319:118074. <https://doi.org/10.1016/j.jmatprotec.2023.118074>
129. Wang J, Xu J, Lu Y, Xie T, Peng J, Chen J (2023) Online supervisory system based on machine vision for laser solid forming. *Micromachines-Basel*, p 14. <https://doi.org/10.3390/mi14081558>
130. Chen Y, Guo Y, Xu M, Ma C, Zhang Q, Wang L, Yao J, Li Z (2019) Study on the element segregation and laves phase formation in the laser metal deposited IN718 superalloy by flat top laser and gaussian distribution laser. *Mater Sci Eng: A* 754:339–347. <https://doi.org/10.1016/j.msea.2019.03.096>
131. Shang S, Wellburn D, Sun YZ, Wang SY, Cheng J, Liang J, Liu CS (2014) Laser beam profile modulation for microstructure control in laser cladding of a NiCrBSi alloy. *Surf Coat Technol* 248:46–53. <https://doi.org/10.1016/j.surfcoat.2014.03.018>
132. Bi J, Wu L, Li S, Yang Z, Jia X, Starostenkov MD, Dong G (2023) Beam shaping technology and its application in metal laser additive manufacturing: a review. *J Mater Res Technol* 26:4606–4628. <https://doi.org/10.1016/j.jmrt.2023.08.037>
133. Fathi A, Khajepour A, Durali M, Toyserkani E (2008) Geometry control of the deposited layer in a nonplanar laser cladding process using a variable structure controller. *J Manuf Sci Eng*. <https://doi.org/10.1115/1.2823085>
134. Devesse W, De Baere D, Guillaume P (2014) Design of a model-based controller with temperature feedback for laser cladding. *Physics Procedia* 56:211–219. <https://doi.org/10.1016/j.phpro.2014.08.165>
135. Ma M, Xiong W, Lian Y, Han D, Zhao C, Zhang J (2020) Modeling and optimization for laser cladding via multi-objective quantum-behaved particle swarm optimization algorithm. *Surf Coat Technol* 381:125129. <https://doi.org/10.1016/j.surfcoat.2019.125129>
136. Yu J, Sun W, Huang H, Wang W, Wang Y, Hu Y (2019) Crack sensitivity control of nickel-based laser coating based on genetic algorithm and neural network. *COATINGS* 9:728. <https://doi.org/10.3390/coatings9110728>
137. Yang S, Bai H, Li C, Shu L, Zhang X, Jia Z (2022) Numerical simulation and multi-objective parameter optimization of Inconel718 coating laser cladding. *Coatings* 12:708. <https://doi.org/10.3390/coatings12050708>
138. Zhou Z, Du Y, He G, Xu L, Shu L (2023) Optimization and characterization of laser cladding of 15-5PH coating on 20Cr13 Stainless Steel. *J MATER ENG PERFORM* 32:962–977. <https://doi.org/10.1007/s11665-022-07157-w>
139. Zhang Y, Xu Y, Sun Y, Cheng W (2022) Surface quality optimization of laser cladding based on surface response and genetic neural network model. *Surf Topogr Metrol Prop* 10:044007. <https://doi.org/10.1088/2051-672X/aca3bd>
140. Peng S, Li T, Zhao J, Lv S, Tan GZ, Dong M, Zhang H (2019) Towards energy and material efficient laser cladding process: modeling and optimization using a hybrid TS-GEP algorithm and the NSGA-II. *J CLEAN PROD* 227:58–69. <https://doi.org/10.1016/j.jclepro.2019.04.187>
141. Deng Z, Chen T, Wang H, Li S, Liu D (2020) Process parameter optimization when preparing Ti (C, N) ceramic coatings using laser cladding based on a neural network and quantum-behaved particle swarm optimization algorithm. *Appl Sci* 10:6331. <https://doi.org/10.3390/app10186331>

142. Gunasegaram DR, Barnard AS, Matthews MJ, Jared BH, Andreaco AM, Bartsch K, Murphy AB (2024) Machine learning-assisted in-situ adaptive strategies for the control of defects and anomalies in metal additive manufacturing. *ADDIT MANUF* 81:104013. <https://doi.org/10.1016/j.addma.2024.104013>
143. Pandiyan V, Cui D, Richter RA, Parrilli A, Leparoux M (2023) Real-time monitoring and quality assurance for laser-based directed energy deposition: integrating co-axial imaging and self-supervised deep learning framework. *J INTELL MANUF*. <https://doi.org/10.1007/s10845-023-02279-x>
144. Miao L, Xing F, Chai Y (2023) Closed loop control of melt pool width in laser directed energy deposition process based on PSO-LQR. *IEEE Access* 78170–78181. <https://doi.org/10.1109/ACCESS.2023.3292789>
145. Chen L, Yao X, Chew Y, Weng F, Moon SK, Bi G (2020) Data-driven adaptive control for laser-based additive manufacturing with automatic controller tuning. *Appl Sci* 10:7967. <https://doi.org/10.3390/app10227967>
146. Farshidianfar MH, Khajepour A, Zeinali M, Gelrich (2013) A System identification and height control of laser cladding using adaptive neuro-fuzzy inference systems, International Congress on Applications of Lasers & Electro-Optics, Laser Institute of America, 615–623. <https://doi.org/10.2351/1.5062940>
147. Chen H, Huang S (2004) Ti6Al4V laser alloying process control by using a self-organizing fuzzy controller. *Int J Mach Tools Manuf* 44:1653–1665. <https://doi.org/10.1016/j.ijmactools.2004.05.002>
148. Li B, Zhang Y, Lei Y, Wei H, Chen C, Liu F, Zhao P, Wang K (2024) A single-sensor multi-scale quality monitoring methodology for laser-directed energy deposition: example with height instability and porosity monitoring in additive manufacturing of ceramic thin-walled parts. *ADDIT MANUF* 79:103923. <https://doi.org/10.1016/j.addma.2023.103923>
149. Xia Y, Qin Y, Zhai D, Chai S (2016) Further results on cloud control systems. *Sci China Inform Sci* 59:1–5. <https://doi.org/10.1007/s11432-016-5586-9>
150. Răileanu S, Anton F, Borangiu T, Anton S, Nicolae M (2018) A cloud-based manufacturing control system with data integration from multiple autonomous agents. *COMPUT IND* 102:50–61. <https://doi.org/10.1016/j.compind.2018.08.004>
151. Chen L, Bi G, Yao X, Tan C, Su J, Ng NPH, Chew Y, Liu K, Moon SK (2023) Multisensor fusion-based digital twin for localized quality prediction in robotic laser-directed energy deposition. *Robot Cim-Int Manuf* 84:102581. <https://doi.org/10.1016/j.rcim.2023.102581>

Publisher's Note Springer Nature remains neutral with regard to jurisdictional claims in published maps and institutional affiliations.

Springer Nature or its licensor (e.g. a society or other partner) holds exclusive rights to this article under a publishing agreement with the author(s) or other rightsholder(s); author self-archiving of the accepted manuscript version of this article is solely governed by the terms of such publishing agreement and applicable law.